



1 Effect of rock uplift and Milankovitch timescale variations in 2 precipitation and vegetation cover on catchment erosion rates

3 Hemanti Sharma¹, Todd A Ehlers^{1*}, Christoph Glotzbach¹, Manuel Schmid¹ Katja Tielbörger²

4 ¹Department of Geosciences, University of Tübingen, 72076 Tübingen, Germany

5 ²Department of Biology, Plant Ecology Group, University of Tübingen, Auf der Morgenstelle 5, 72076 Tübingen, Germany

6 *Correspondence to:* Todd A. Ehlers (todd.ehlers@uni-tuebingen.de)

7 **Abstract.** Catchment erosion and sedimentation are influenced by variations in the rates of rock uplift (tectonics), and periodic
8 fluctuations in climate and vegetation cover. In this study we applied the Landlab-SPACE landscape evolution modelling
9 approach. This study focuses on quantifying the effects changing climate and vegetation on erosion and sedimentation over
10 distinct climate-vegetation settings. As catchment evolution is subjected to tectonic and climate forcings at millennial to
11 million-year time-scales, the simulations are performed over different tectonic scenarios and periodicities of climate-vegetation
12 change. We present a series of generalized experiments that explore the sensitivity of catchment hillslope and fluvial erosion
13 and sedimentation for different rock uplift rates (0.05 mm a⁻¹, 0.1 mm a⁻¹, 0.2 mm a⁻¹) and Milankovitch climate periodicities
14 (23 kyr, 41 kyr and 100 kyr). Model inputs were parameterized for two different climate and vegetation conditions at two sites
15 in the Chilean Coastal Cordillera at ~26°S (arid and sparsely vegetated) and ~33°S (mediterranean). For each setting, steady
16 state topographies were produced for each uplift rate before introducing periodic variations in precipitation and vegetation
17 cover. Following this, the sensitivity of these landscapes was analysed for 3 Myr in a transient state. Results suggest that
18 regardless of the uplift rate, transients in precipitation and vegetation cover resulted in transients in erosion rates in the direction
19 of change in precipitation and vegetation. While the transients in sedimentation were observed to be in the opposite direction
20 of change in the precipitation and vegetation cover, with phase lags of ~1.5 – 2.5 kyr. These phase lags can be attributed to the
21 changes in plant functional type (PFT) distribution induced by the changes in climatic conditions, which is beyond the scope
22 of this study. These effects being most pronounced over longer period changes (100 kyr) and higher rock uplift rates (0.2 mm
23 yr⁻¹). This holds true for both vegetation and climate settings. Furthermore, transient changes in catchment erosion due to
24 varying vegetation and precipitation were between ~35%-110% of the background (rock uplift) rate and are measureable with
25 some techniques (e.g. sediment flux histories, cosmogenic nuclides). Taken together, we find that vegetation-dependent
26 erosion and sedimentation are influenced by Milankovitch timescale changes in climate, but that these transient changes are
27 superimposed upon tectonically driven rates of rock uplift.

28 **Keywords:** vegetation dynamics, climate change, tectonics, landscape evolution modelling, SPACE, Landlab

29 1 Introduction

30 The pioneering work of G.K. Gilbert (Gilbert, 1877) highlighted that surface uplift, climate, and biota (amongst other things)
31 jointly influence catchment-scale rates of weathering and erosion. In recent decades a wide range of studies have built upon
32 these concepts and quantified different ways in which climate, tectonics, or vegetation cover influence rates of erosion and
33 sedimentation. For example, recent work highlights that higher vegetation and lower precipitation both decrease erosion
34 (Alonso et al., 2006; Bonnet and Crave, 2003; Huntley et al., 2013; McPhillips et al., 2013; Miller et al., 2013; Perron, 2017;
35 Schaller et al., 2018; Starke et al., 2020; Tucker, 2004). In addition, periodic changes in climate (such as changes driven by
36 Milankovitch timescale orbital variations) have also been recognized as influencing rates of catchment erosion and
37 sedimentation (Braun et al., 2015; Hancock and Anderson, 2002; Hyun et al., 2005; Schaller et al., 2004) although our ability
38 to measure orbital timescale induced erosional changes can be challenging (e.g. Schaller and Ehlers, 2006; Whipple, 2009).
39 Several studies have also documented how the combined effects of either climate and vegetation change, or variable rates of



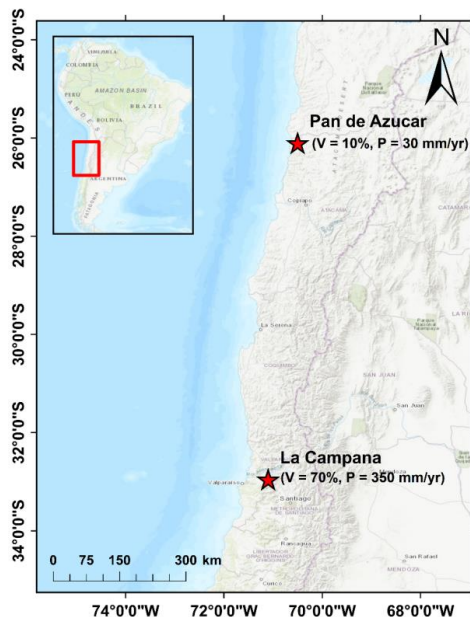
40 rock uplift and climate change (including glaciation) impact catchment scale processes (Herman et al., 2010; Mishra et al.,
41 2019; Schmid et al., 2018; Tucker, 2004; Yanites and Ehlers, 2012). Taken together, the previous studies have found that the
42 long-term development of topography (such as over million-year time scales) is in many situations sensitive to the tectonic,
43 climate, and vegetation history of the region, and that competing effects of different coeval processes (e.g. climate change and
44 tectonics) exist, but are not well understood. In this study, we build upon these concepts to test two hypotheses related to the
45 sensitivity of catchment erosion and sedimentation to the combined effects for different rock uplift rates and Milankovitch
46 time scale variations in precipitation and vegetation cover. First, we evaluate if vegetation cover and climate vary on
47 Milankovitch timescales, then any increases or decreases in catchment erosion will be more pronounced over longer (e.g. 100
48 kyr) rather than shorter (e.g. 21 kyr) periodicities due to the longer duration of any climate or vegetation change occurring at
49 longer periodicities. Second, if increasing rates of tectonic uplift cause increases in catchment erosion rates, then any periodic
50 variations in climate and vegetation cover will be muted (lower amplitude) at higher uplift rates as the effect of rock uplift
51 outweigh climate and vegetation changes. Given the complexity of this problem, we do evaluate these hypotheses through
52 numerical landscape evolution modelling using a step-wise increase in model complexity where the contributions of individual
53 processes (i.e. climate, or vegetation, or tectonics) are identified separately before looking into the fully coupled system and
54 resulting interactions.

55 Quantification of climate, vegetation, and tectonic effects on catchment erosion is challenging because these processes are
56 confounded and can, if coupled, have opposing effects on erosion and/or sedimentation. For example, precipitation has both
57 direct (positive) as well as indirect effects on erosion that operate via vegetation cover. Namely, plants require water to grow
58 and survive, vegetation cover is usually positively affected by precipitation both on a global scale (i.e. when comparing biomes
59 across latitudinal gradients) as well as on a regional or local scale (e.g. Huxman et al., 2004; Sala et al., 1988; Zhang et al.,
60 2016). Though vegetation cover is also influenced by temperature, seasonality and many other abiotic factors such as soils,
61 the positive relationship of biomass and cover with water availability is rather general. For example, in dry ecosystems such
62 as hot deserts or Mediterranean systems, vegetation cover is primarily limited by water availability and is therefore very low.
63 As precipitation increases, vegetation cover increases rapidly, and other factors become limiting (Breckle, 2002). In temperate
64 systems, where water is abundant and soils well developed, plant growth is primarily limited by low winter temperatures.
65 Overall, the relationship between precipitation and vegetation cover follows a saturation curve with large sensitivity (e.g.
66 measured as rain use efficiency- RUE) to precipitation in arid to Mediterranean systems and low sensitivity in temperate or
67 tropical systems (Gerten et al., 2008; Huxman et al., 2004; Yang et al., 2008).

68 Previous modelling and observational studies have made significant progress in understanding the interactions between surface
69 processes and either climate (Dixon et al., 2009; Routschek et al., 2014; Seybold et al., 2017; Slater and Singer, 2013),
70 vegetation (Acosta et al., 2015; Amundson et al., 2015; Istanbuluoglu, 2005) or coupled climate-vegetation dynamics (Dosseto
71 et al., 2010; Jeffery et al., 2014; Mishra et al., 2019; Schmid et al., 2018). Over geologic (millennial to million-year) timescales,
72 observational studies of these interactions are impossible (or require proxy data) and numerical approaches provide an ideal
73 means to explore interactions between climate, vegetation, tectonics, and topography. The first observational study of this kind
74 suggested that high MAP (mean annual precipitation) is associated with denser vegetation and hence resulting in lower erosion
75 rates (Langbein and Schumm, 1958). One of the first numerical modeling studies implementing a vegetation-erosion coupling
76 was conducted by Collins et al. (2004). This study was followed by work from Istanbuluoglu and Bras (2006), which
77 quantified the effect of vegetation on landscape relief and drainage formation. More recently, work by Schmid et al. (2018)
78 included the effects of transient climate and vegetation coupled with a landscape evolution model to predict topographic and
79 erosional variations over millennial- to million-year timescales. However, Schmid et al., (2018) presented a simplified
80 approach to consider hillslope and detachment-limited fluvial erosion and only considered a homogeneous substrate. Other
81 studies have documented that sediment or bedrock erosion by rivers is not dominated purely by detachment-limited (Howard,
82 1994) or transport-limited fluvial erosion (Willgoose et al., 1991). Rather, it often involves a combination of, or transition



83 between, both conditions (e.g., Pelletier, 2012). Given this, treatment of bedrock erosion and sediment transport for mixed
84 bedrock-alluvial streambeds provides a more realistic framework for understanding the influence of climate, vegetation, and
85 tectonic processes on topographic development. Recent work (Shobe et al., 2017) presented an additional component (SPACE)
86 to the Landlab surface process model modified by Schmid et al. (2018). SPACE allows for the simulation of mixed detachment-
87 transport limited fluvial processes, including separate layers for bedrock and loose sediment. Finally, the sensitivity of
88 topography to different rock uplift rates in variable climate-vegetation settings has not yet been investigated. The combined
89 interactions of tectonics (rock uplift) and variable climate and vegetation warrant investigation given the significant influence
90 of rock uplift on mean elevation, erosion rates and river channel profiles (Kirby and Whipple, 2012; Turowski et al., 2006)
91 and hillslopes.



92
93 **Figure 1:** The representative study areas in the Chilean Coastal Cordillera used for the model setup (ESRI 2019). The model
94 parameters were loosely tuned to the climate and vegetation conditions in these areas (Schmid et al., 2018). The Pan de Azucar area
95 in the north neighbours the Atacama Desert and has sparse vegetation cover (10%) and an arid climate (30 mm yr⁻¹). The La
96 Campana area in south has a Mediterranean climate and ecosystem with more abundant vegetation (70%) and precipitation (350
97 mm yr⁻¹). These two study areas are part of the German EarthShape priority research program (www.earthshape.net).

98 In this study, we complement the previous work and investigate the transient landscape response for mixed bedrock-alluvial
99 systems. We do this for different rates of rock uplift and periodic changes (Milankovitch cycles) in precipitation and vegetation.
100 Our focus is on erosion and sedimentation changes occurring over millennial to million-year timescales. Sub-annual to decadal
101 scale changes are beyond the scope of this study. Our approach involves a two-dimensional coupled detachment-transport
102 limited landscape evolution model for fluvial processes. In addition, hillslope diffusion (Johnstone and Hillel, 2014) and
103 weathering and soil production (Ahnert, 1977) processes are considered. Although this study is primarily focused on
104 documenting the predicted sensitivity of catchments to variations in tectonics, climate, and vegetation change – we have tuned
105 our model setup to the conditions along the Chilean Coastal Cordillera (Fig. 1) which features a similar tectonic setting, but
106 an extreme climate and ecological gradient. This was done to provide realistic parameterizations for vegetation cover and
107 precipitation in different ecological settings. This area is also part of the German-Chilean priority research program,
108 *EarthShape: Earth Surface Shaping by Biota* (www.earthshape.net) where extensive ongoing research is occurring.



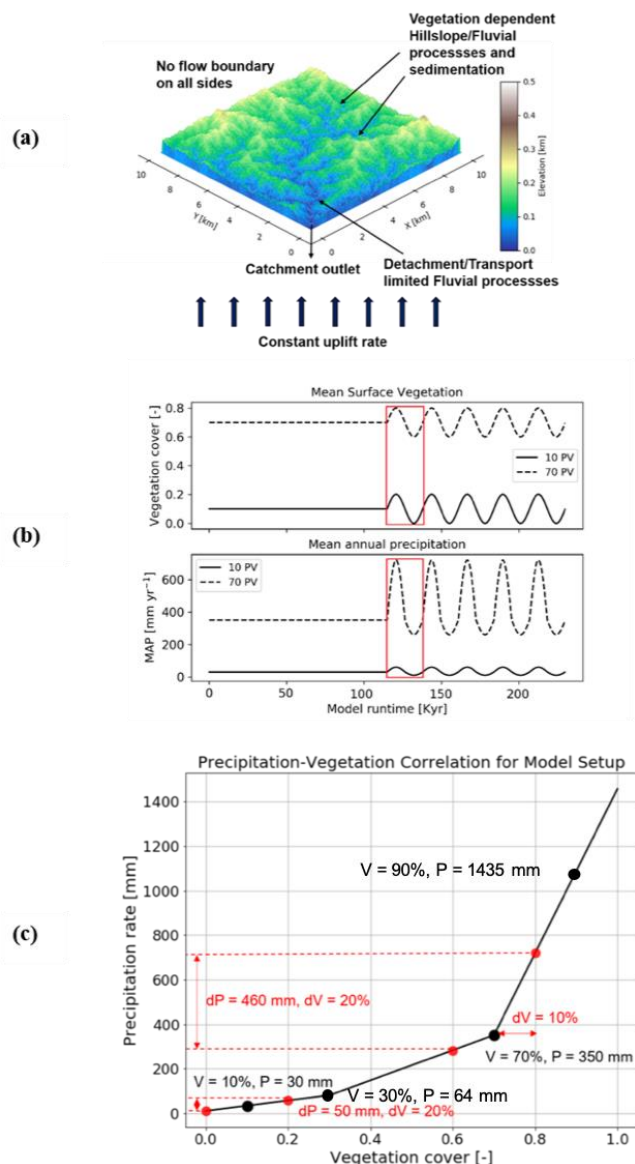
109 **2 Methods**

110 We apply the landscape evolution model, Landlab (Hobley et al., 2017) using the SPACE 1.0 module of Shobe et al. (2017)
111 for detachment vs. transport limited fluvial processes. The Landlab/SPACE programs were modified for vegetation dependent
112 hillslope and fluvial erosion using the approach of Schmid et al. (2018). In general, the geomorphic processes considered
113 involve weathering and regolith production calibrated to the Chilean Coastal Cordillera observations of Schaller et al. (2018),
114 vegetation dependent coupled detachment-transport limited fluvial erosion, and depth dependent hillslope diffusion. The model
115 parameters (i.e., bedrock and sediment erodibility and diffusion coefficient) in the simulations are based on those of Schmid
116 et al. (2018). A detailed explanation of the weathering, erosion, sediment transport and deposition processes is provided in
117 Appendix A, and a summary of model parameters used is given in Table 1.

118 **2.1 Model setup and scenarios considered**

119 The model consists of a 10 km by 10 km rectangular grid with 100 m node spacing (Fig. 2a), with a total domain area of 100
120 km². We conducted generalized simulations that are loosely tuned to the climate and vegetation conditions in two areas in
121 the Chilean Coastal Cordillera (Fig. 1) which have predominantly granitoid lithology (van Dongen et al., 2018; Kojima et al.,
122 2017; Oeser et al., 2018; Rossel et al., 2018). These areas exhibit a large climate and vegetation gradient ranging from and
123 arid climate (MAP: 30 mm) and sparse vegetation (10%) in Pan de Azucar National Park to a wetter Mediterranean climate
124 (MAP: 35 cm) with more abundant vegetation (70%) in La Campana National Park.

125 Bedrock elevation and sediment cover thickness are considered as separate layers to quantify simultaneous bedrock erosion
126 and sediment entrainment across the model domain. Simulations were conducted for 15 Myr to generate a steady-state
127 topography with the mean values of precipitation and vegetation cover for the two study areas. The rates of rock uplift are kept
128 constant during the steady-state simulations, and subsequently in the transient stage with oscillating vegetation cover and
129 precipitation. After the development of a steady-state topography, transient forcings in vegetation cover and mean annual
130 precipitation (MAP) (Fig. 2b) were introduced for 3 Myr. Vegetation cover varied by $\pm 10\%$ around the mean value used to
131 develop the steady-state topography. The 10% vegetation cover variation is based on the dynamic vegetation modelling results
132 of Werner et al. (2018) for the Chilean Coastal Cordillera. They found that from the Last Glacial Maximum to present that
133 vegetation cover in the region varied by $\sim 10\%$. The periodicity of vegetation change varied between simulations (Table 1).
134 Changes in vegetation cover are driven by climatic variations, where MAP has been shown to be much more influential than
135 temperature changes, especially in relatively dry regions (e.g. Mowll et al., 2015) and in grasslands (e.g. Sala et al., 1988).
136 Many previous studies have shown that annual primary production (ANPP) and associated vegetation cover increases linearly
137 (Mowll et al., 2015; Xia et al., 2014) or in an asymptotic manner with MAP (Huxman et al., 2004; Smith et al., 2017; Yang et
138 al., 2008; Zhang et al., 2016). These findings are also highly consistent among different approaches such as global (Gerten et
139 al., 2008) or regional (Zhang et al., 2016) models, field and remotely-sensed observations across biomes and among years
140 (Huxman et al., 2004; Xia et al., 2014; Yang et al., 2008), as well as rapid vegetation responses to rainfall manipulation
141 experiments (Smith et al., 2017). An asymptotic relationship appears the more common case, especially when looking at warm
142 and dry ecosystems, i.e. regions up to approx. 600mm MAP (Huxman et al., 2004; Mowll et al., 2015). Here, it has been
143 demonstrated that the sensitivity of ANPP to MAP decreases from more water-limited systems such as deserts to
144 Mediterranean and temperate regions (Huxman et al., 2004; Yang et al., 2008). Namely, the same increase in MAP will yield
145 much larger increases in vegetation cover in dry regions than in wetter ones. To implement these effects, we use an empirical
146 approach based on vegetation-precipitation relationships observed in the Chilean Coastal Cordillera (see Schmid et al. 2018
147 for details) to estimate what mean annual precipitation rates are associated with different vegetation cover amounts (Fig. 2b,
148 2c).



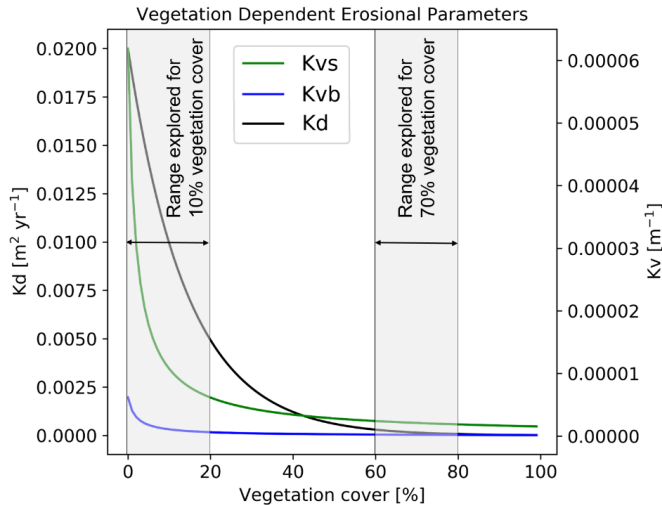
149

150 **Figure 2: Model geometry and climate and vegetation forcings used in this study.** (a) A simple representation of the model setup
 151 with a square grid, and catchment outlet in the lower left corner. (b) Graphical representation of the magnitude and pattern of
 152 fluctuations imposed on vegetation (top) and precipitation (bottom) during the transient state of the model. Red rectangles
 153 represent one cycle, whose effects are discussed in detail. (c) Graphical representation of precipitation and vegetation cover
 154 correlation from the Chilean study areas and used as the empirical bases for how precipitation rates vary for +/-10% changes in
 155 vegetation cover (Schmid et al., 2018).

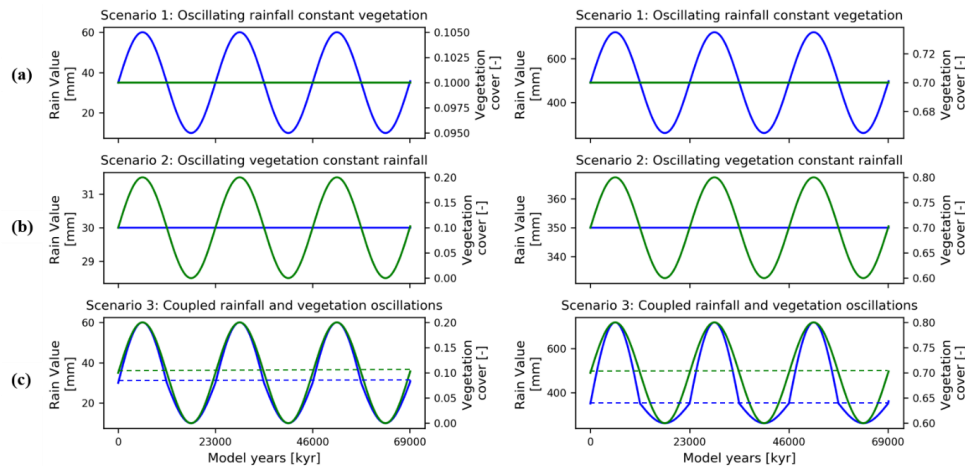
156 The effects of vegetation cover on hillslope and fluvial processes are modified from the approach of Schmid et al, (2018), see
 157 also Appendix, and Table 1. Briefly, we applied a slope and depth-dependent linear diffusion rule following the approach of
 158 Johnstone and Hillel (2014). The diffusion coefficient (K_d) is defined as a function of the bare soil diffusivity (K_b) and
 159 exponentially varies with vegetation cover following the approach of Istanbuluoglu (2005) and Dunne et al. (2010). Fluvial
 160 erosion is estimated for a two-layer topography (i.e., bedrock and sediment are treated explicitly) in the coupled detachment –
 161 transport limited model. Bedrock erosion and sediment entrainment are calculated simultaneously in the model following the
 162 approach of Shobe et al. (2017). The effects of vegetation cover on fluvial erosion were implemented using the approach of



163 Istanbuluoglu (2005) and Schmid et al. (2018) and by introducing the effect of a vegetation dependent Manning’s roughness.
 164 The sediment and bedrock erodibility (K_{vs} and K_{vb} , respectively) are influenced by the fraction of vegetation cover V (see
 165 appendix for governing equations). Fig. 3 shows the range of resulting diffusion coefficients (K_d) and sediment and bedrock
 166 erodibility (K_{vs} , K_{vb} , respectively) values considered in this study. The exponential and power-law relationships producing
 167 these values, respectively, are a source of non-linearity that are manifested in the results discussed in subsequent sections.



168
 169 **Figure 3:** Graphical representation of the range of vegetation dependent diffusion coefficient (K_d , left y-axis), sediment erodibility
 170 (K_{vs}), and bedrock erodibility (K_{vb}) values considered in this study (see Appendix for governing equations). The combined
 171 erodibility is referred to as K_v (right y-axis).



172
 173 **Figure 4:** Graphical representation of the different precipitation and vegetation forcings applied to the model scenarios described
 174 in the text. Forcings for sparse vegetation (10%) cover are shown on the left, and dense vegetation (70%) cover on the right. Scenarios
 175 explored include: (a) Oscillating precipitation and constant vegetation cover. (b) Oscillating vegetation and constant precipitation.
 176 (c) Coupled oscillations in precipitation and vegetation cover.

177 As the study areas exhibit similar granitoid lithology, the erosional parameters (Table. 1) are kept uniform for both the study
 178 areas. However, parameters based on climate conditions namely soil production rate (Schaller et al., 2018), MAP and
 179 vegetation cover (Schmid et al., 2018), are different for these areas. The vegetation cover and precipitation rate are kept uniform
 180 across the model domain due to low to moderate relief in target catchments (~750 m for Pan de Azucar and ~1500 m in La
 181 Campana).



- 182 The model scenarios considered were designed to provide a stepwise increase in model complexity to identify how variations
 183 in precipitation, vegetation cover, or rock uplift rate influence erosion and sedimentation. The model scenarios include:
 184 1. Influence of oscillating precipitation and constant vegetation cover, on erosion and sedimentation (Fig. 4a, Fig. 5, Section
 185 3.1).
 186 2. Influence of constant precipitation and oscillating vegetation cover, on erosion and sedimentation (Fig. 4b, Fig. 6, Section
 187 3.2).
 188 3. Influence coupled oscillations in precipitation and vegetation cover, on erosion and sedimentation (Fig. 4c, Fig. 7, Section
 189 3.3).
 190 4. Influence of different periodicities of precipitation/vegetation change on erosion and sedimentation (Fig. 8, Section 3.4).
 191 5. Influence of rock uplift rate and oscillating precipitation/vegetation on erosion sedimentation (Fig. 9, Section 3.5).

192 **Table 1. Landscape evolution model input parameters used and corresponding units.**

Model Parameters	Values
Grid size	10 [km] x 10 [km], dx: 100 [m]
Model runtime (totalTime)	Steady-state: 15 [Ma], Transient state: 3 [Ma]
Rock uplift rates (U)	0.05 [mm a ⁻¹], 0.1 [mm a ⁻¹], 0.2 [mm a ⁻¹]
Periodicities (sinePeriod)	23 [kyr], 41 [kyr], 100 [kyr] (Milankovitch cycles)
Initial sediment thickness (H _{initial})	0 [m]
Bedrock erodibility (Kr)	2 x 10 ⁻⁹ [m ⁻¹]
Sediment erodibility (Ks)	2 x 10 ⁻⁸ [m ⁻¹]
Soil production/transport decay depth (h*)	0.5 [m]
Reach scale bedrock roughness (H*)	1 [m]
Porosity (φ)	0.2 [-]
Fraction of fine sediments (Ff)	0.2 [-]
Effective terminal settling velocity (Vs)	10 [m a ⁻¹]
m, n	0.6, 1 [-]
Bedrock erosion threshold stream power (ω _{cr})	5 x 10 ⁻⁴ [m a ⁻¹]
Sed. entr. threshold stream power (ω _{cs})	5 x 10 ⁻⁵ [m a ⁻¹]
Maximum sediment production rate (W _o)	9.7 x 10 ⁻⁶ [m yr ⁻¹] (10% Veg. cover), 1.3 x 10 ⁻⁴ [m yr ⁻¹] (70% Veg. cover)
Mean annual precipitation (P)	0.03 [m yr ⁻¹] (10% Veg. cover), 0.35 [m yr ⁻¹] (70% Veg. cover)
Bare soil diffusivity (K _b)	0.01 [m ² yr ⁻¹]
Exponential decay coefficient (α)	0.3 [-]
Critical channel formation area (A _{crit})	1 x 10 ⁶ [m ²]
Reference vegetation cover (V _r)	1 (100%)
Manning's number for bare soil (n _s)	0.01 [-]
Manning's number for ref. vegetation (n _v)	0.6 [-]
Scaling factor for vegetation influence (w)	1 [-]

193 The rate of rock uplift is kept temporally and spatially constant (0.05 mm a⁻¹) for both study areas, for the simulations in
 194 scenarios 1 – 4. This is done in order to minimize the effect of tectonics on topography to isolate the sensitivity of geomorphic
 195 processes to changing precipitation and vegetation cover. In scenario 5, the effect of different rock uplift rates (i.e., 0.05 mm
 196 a⁻¹, 0.1 mm a⁻¹ and, 0.2 mm a⁻¹) is studied in combination with the coupled oscillations in precipitation and vegetation cover.



197 The rock uplift rate used in the scenarios 1 – 4 is influenced by the findings of Melnick (2016) and Avdievitch et al. (2018),
198 which suggests the modern and paleo uplift and exhumation rates of $< 0.1 \text{ mm a}^{-1}$ for the study areas and northern Coastal
199 Cordillera in general. Similarly, the periodicity of oscillations for precipitation and vegetation cover are kept constant (23 kyr)
200 for model scenarios 1, 2, 3, and 5. In scenario 4, the effect of different periodicities (i.e., 23 kyr, 41kyr, and 100 kyr) is studied
201 in combination with coupled oscillations in precipitation and vegetation cover. The periodicities of oscillations are based on
202 Milankovitch cycles (Ashkenazy et al., 2010; Hyun et al., 2005).

203 2.2 Boundary and Initial conditions

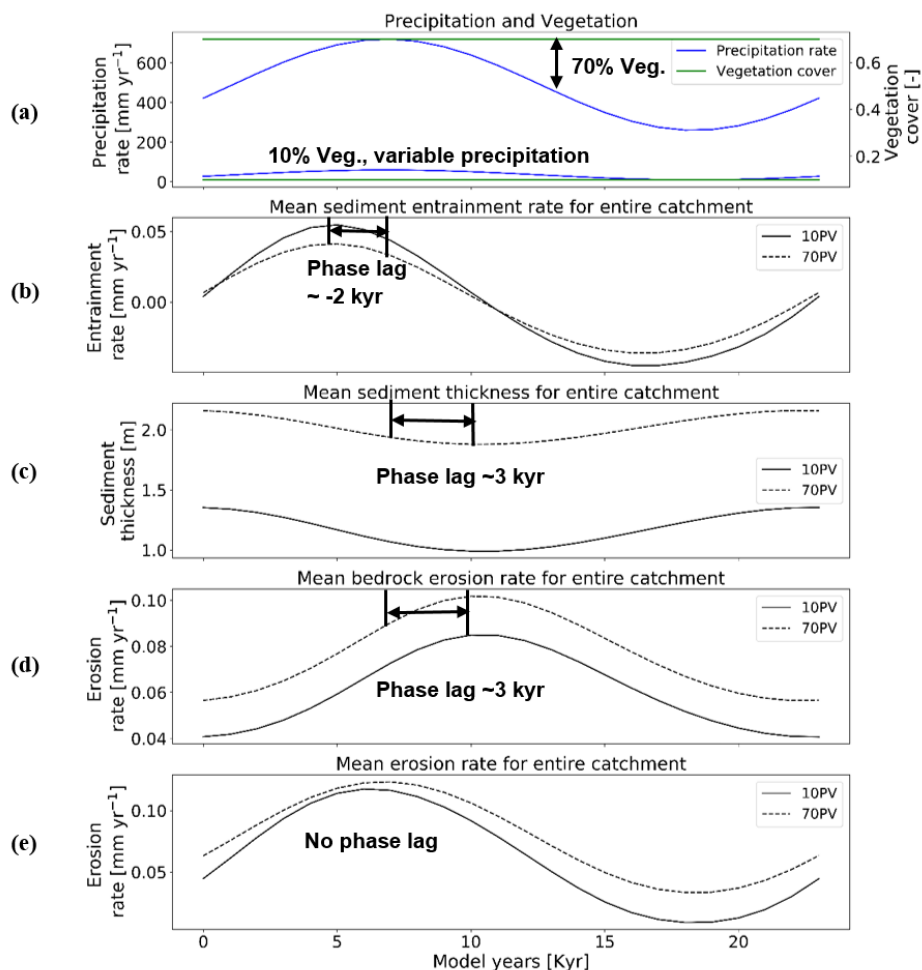
204 An initial low relief ($< 1 \text{ m}$) random noise topography was applied to the model grid at the start of the simulations. The initial
205 topographies had a slight initial topographic slope of $\approx 1.4 \times 10^{-5}$ (Fig. 2a). The boundaries on all sides of the domain were
206 closed (no flow), except the south-west corner node which was an outlet node. From these conditions, the steady-state
207 topography was calculated over 15 Myr model time, and the resulting bedrock elevation and sediment thickness were used as
208 input for the transient scenarios described in section 2.1.

209 3 Results

210 In the following sections, we focus our analysis on the mean catchment sediment thickness (i.e. the combined thickness of soil
211 and regolith) over then entire domain, mean bedrock erosion rates (excluding sediment erosion), mean sediment entrainment
212 rates and the mean (or net) catchment erosion rates. The mean catchment erosion rates are the sum of bedrock erosion and
213 sediment entrainment rates. To simplify the presentation of result, results are shown only for the first cycle of transient climate
214 and vegetation change. Results from the first cycle were representative of subsequent cycles (not shown), and no longer-term
215 variations or trends in erosion/sedimentation were identified or warrant discussion.

216 3.1 Influence of oscillating precipitation and constant vegetation cover on erosion and sedimentation (Scenario 1)

217 In this scenario, with a rock uplift rate of 0.05 mm a^{-1} and 23kyr periodicity in precipitation, the mean catchment sediment
218 entrainment rates follow the pattern of change in precipitation (Fig. 5a, b), but with an offset (phase lag) between the maxima
219 and minima of entrainment. A higher variation in the range of sediment entrainment rates (i.e., $-0.036 \text{ mm yr}^{-1} - 0.043 \text{ mm}$
220 yr^{-1} , Fig. 5b) is observed for simulations with 10% vegetation cover. Negative values in sediment entrainment rates corresponds
221 to sediment deposition rates during drier periods. The peak in sediment entrainment rates (e.g. 0.043 mm yr^{-1} for 10% veg.,
222 and $\sim 0.038 \text{ mm yr}^{-1}$ for 70% veg., Fig. 5b), is observed with a time lag of ($\sim -2 \text{ kyr}$) before the peak in maximum precipitation
223 in both the 10% and 70% vegetation cover simulations. This result suggests that as precipitation increases sediment is readily
224 entrained where available in the catchment until bedrock is locally exposed. The changes in mean catchment sediment
225 thickness (Fig. 5c) are influenced by changes in the sediment entrainment and precipitation rates, but with a lag time between
226 the maximum in precipitation and the minimum in sediment thickness. The lowest mean catchment sediment thickness (e.g.
227 $\sim 0.97 \text{ m}$ for 10% veg., and $\sim 1.9 \text{ m}$ for 70% veg., Fig. 5c) also occurs with a time lag of ($\sim 3 \text{ kyr}$) after the peak in precipitation
228 rates, for both the 10% and 70% vegetation cover simulations. The same time lag ($\sim 3 \text{ kyr}$) is observed in the peak in mean
229 catchment bedrock erosion (e.g. $\sim 0.087 \text{ mm yr}^{-1}$ for 10% veg. and $\sim 0.1 \text{ mm yr}^{-1}$ for 70% veg., Fig. 5d) and coincides with
230 when the minimum sediment cover is present and more bedrock is exposed for erosion. Finally, the mean-catchment erosion
231 rates follow the pattern of change in precipitation rates (Fig. 5a, 5e) without a phase lag. The maximum erosion rates are similar
232 in range for both the 10% and 70% vegetation cover simulations (e.g. $\sim 0.12 \text{ mm yr}^{-1}$, Fig. 5e). However, in the 10% vegetation
233 cover simulation, the minimum in the mean catchment erosion rate decreases more (e.g. to $\sim 0.01 \text{ mm yr}^{-1}$, Fig. 5e) relative to
234 the higher vegetation cover scenario. The different decreases in the minimum erosion rate between the two vegetation cover
235 amounts corresponds to the differences in precipitation rates (Figs 5a, 4a).



236

237 **Figure 5: Temporal evolution of catchment averaged predictions for scenario 1 described in the text (section 3.1). Graphical**
 238 **representation of mean catchment sedimentation and erosion to (a) oscillating precipitation [mm yr⁻¹] and constant vegetation**
 239 **cover [-] in terms of (b) sediment thickness [m], (c) bedrock erosion [mm yr⁻¹], (d) sediment entrainment [mm yr⁻¹], (e) net**
 240 **erosion rates [mm yr⁻¹] for entire catchment. The periodicity of climate and vegetation oscillations is 23 kyr with rate of rock uplift**
 241 **as 0.5 mm yr⁻¹.**

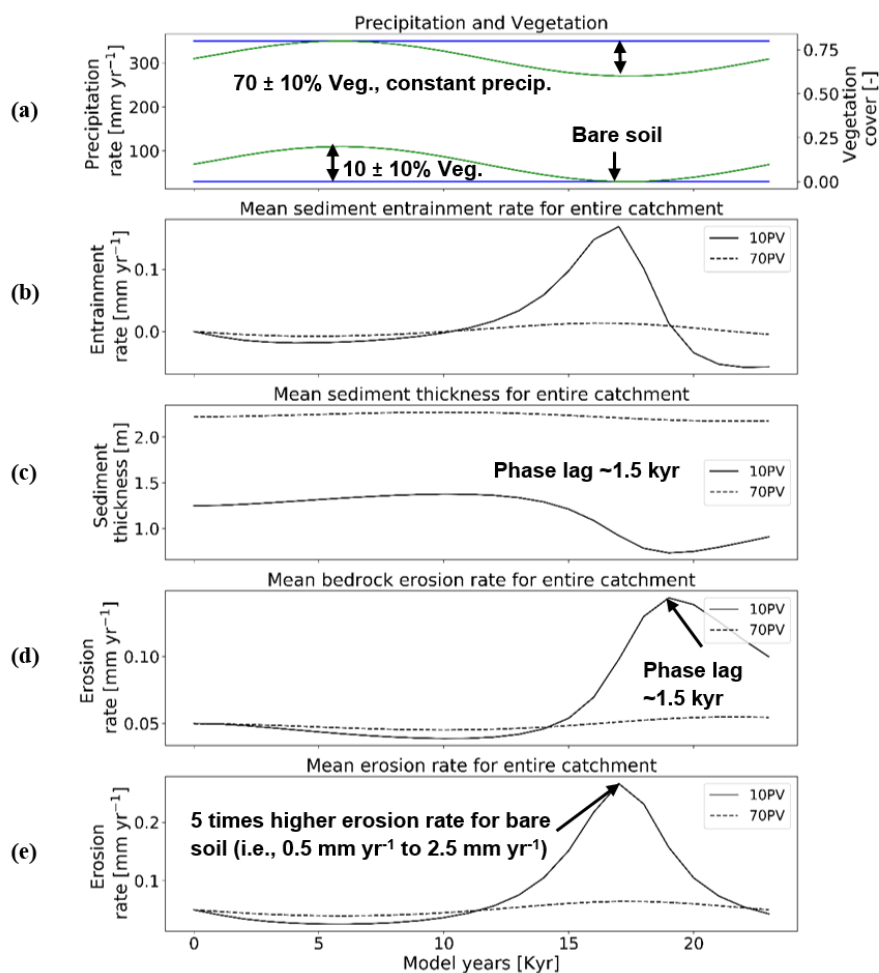
242 The absence of a phase lag between the mean-catchment erosion and precipitation rates reflects that the combined sediment
 243 entrainment and bedrock erosion rates when added together track the overall trend in precipitation rate changes, but the
 244 individual components (sediment vs. bedrock) respond differently.

245 3.2 Influence of constant precipitation, oscillating vegetation cover, on erosion and sedimentation (Scenario 2)

246 Results from this scenario with constant mean annual precipitation (at the mean value of the previous scenario) and oscillating
 247 vegetation cover (Fig. 4b. 6a) show a starkly different catchment response from scenario 1 (section 3.1). The sediment
 248 entrainment rates show for both simulations (Fig. 6b) a small decrease in entrainment as vegetation cover increases (e.g. ~ -
 249 0.05 mm yr⁻¹ for 10% veg., and ~ -0.01 mm yr⁻¹ for 70% veg., Fig. 6b). As vegetation cover decreases later in the cycle,
 250 entrainment rates increase (e.g. to ~0.13 mm yr⁻¹ for 10% veg., and to 0.01 mm yr⁻¹ for 70% veg., Fig. 6b). The larger magnitude
 251 of increase in entrainment for the 10% vegetation cover case corresponds to the minimum (0%) in vegetation cover where the



252 potential for erosion is the highest. In the 10% vegetation cover simulation, the lowest mean catchment sediment thickness
 253 (Fig. 6c was observed ~ 1.5 kyr after the minimum in vegetation cover.



254

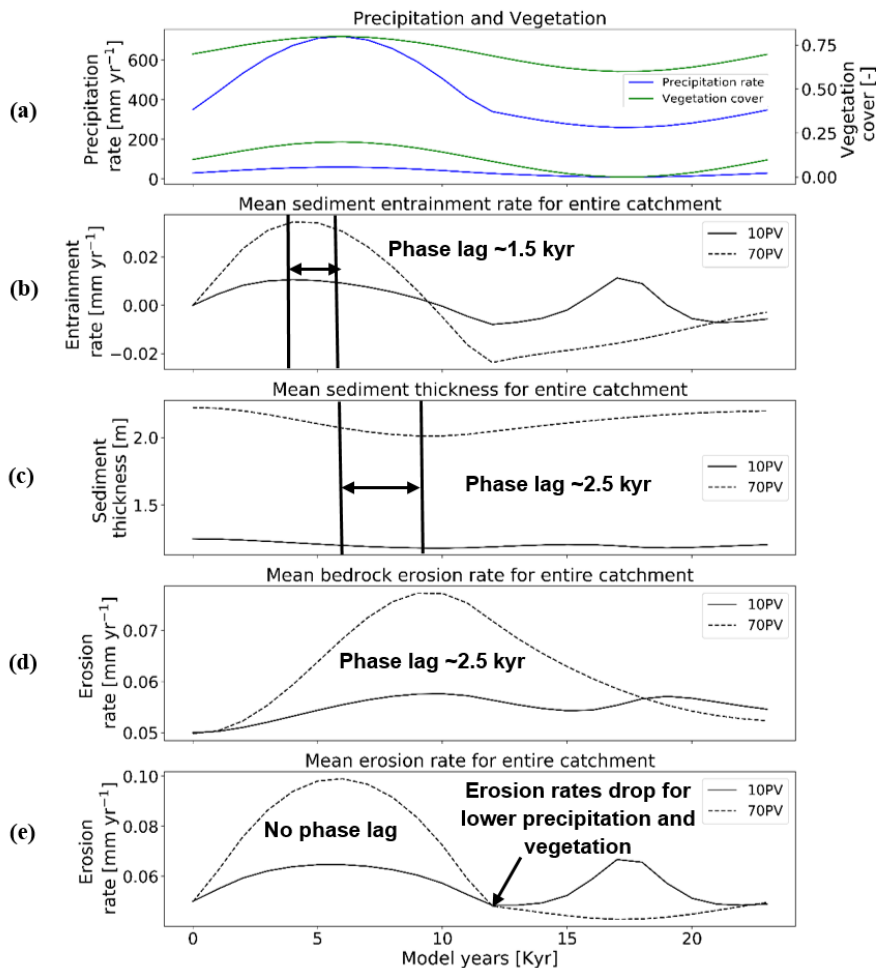
255 **Figure 6:** Temporal evolution of catchment averaged predictions for scenario 2 described in the text (section 3.2). Graphical
 256 representation of mean catchment sedimentation and erosion to (a) constant precipitation [mm yr^{-1}] and oscillating vegetation cover
 257 [-] in terms of (b) sediment thickness [m], (c) bedrock erosion [mm yr^{-1}], (d) sediment entrainment [mm yr^{-1}], (e) net erosion rates
 258 [mm yr^{-1}] for entire catchment. The periodicity of climate and vegetation oscillations is 23 kyr with rate of rock uplift as 0.5 mm yr^{-1} .
 259

260 The range of mean catchment sediment thickness varies significantly in the simulations (e.g. $\sim 0.72 \text{ m} - \sim 1.38 \text{ m}$ for 10% veg.,
 261 and $\sim 2.2 \text{ m} - \sim 2.3 \text{ m}$ for 70% veg., Fig. 6c). The same time lag (~ 1.5 kyr) is observed between the peak in mean catchment
 262 bedrock erosion rates (Fig. 6d) and the minimum in vegetation cover. This is most likely due to the maximum exposure of
 263 bedrock for erosion when catchment average sediment thicknesses are at their minimum. Finally, mean catchment erosion
 264 rates (Fig. 6e) are significantly affected ($\sim +0.26 \text{ mm yr}^{-1}$) by oscillating vegetation cover in simulations with a mean 10%
 265 vegetation. In the 10% vegetation cover simulation, the maximum in erosion rate occurs during the minimum (0%) in
 266 vegetation cover. For the 70% vegetation cover simulation, a similar maximum in erosion occurs also during the minimum in
 267 vegetation, but is far less dramatic, presumably due to the still somewhat large (60%) amount of vegetation-cover present.



268 **3.3 Influence of coupled oscillations of precipitation and vegetation cover, on erosion and sedimentation (Scenario 3)**

269 The catchment response to coupled oscillations in precipitation rate and vegetation cover (Fig. 4c) on erosion and
 270 sedimentation represents a composite of the effects discussed in the previous 2 sections (Fig. 7). For example, the mean
 271 catchment sediment entrainment rates have a peak in entrainment rates (~1.5 kyr) prior to the peak in climate/vegetation values.
 272 A similar effect was noted for scenarios 1 (Fig. 5, section 3.1). As the precipitation rates and vegetation cover decrease later
 273 in the cycle (Fig. 7a), the sediment entrainment rates increase. In more detail, the 70% vegetation cover simulations show a
 274 modest increase similar to that observed in scenario 1 (Fig. 5b), whereas the 10% vegetation cover shows a sharp peak in
 275 the sediment entrainment rates when 0% vegetation cover is present. This later observation is similar what is observed for
 276 scenario 2 (Fig. 6b, section 3.2). Thus, in the case of co-varying precipitation rates and vegetation cover, the response observed
 277 in terms of sediment entrainment is not predicted to be the same for all degrees of vegetation cover, and depends heavily on
 278 the initial vegetation cover of the system around which variations occur.



279

280 **Figure 7: Temporal evolution of catchment averaged predictions for scenario 3 described in the text (section 3.3). Graphical**
 281 **representation of mean catchment sedimentation and erosion to (a) coupled oscillations in precipitation [mm yr⁻¹] and vegetation**
 282 **cover [-] in terms of (b) sediment thickness [-], (c) bedrock erosion [mm yr⁻¹], (d) sediment entrainment [mm yr⁻¹], (e) net erosion**
 283 **rates [mm yr⁻¹] for entire catchment. The periodicity of climate and vegetation oscillations is 23 kyr with rate of rock uplift as 0.5**
 284 **mm yr⁻¹.**



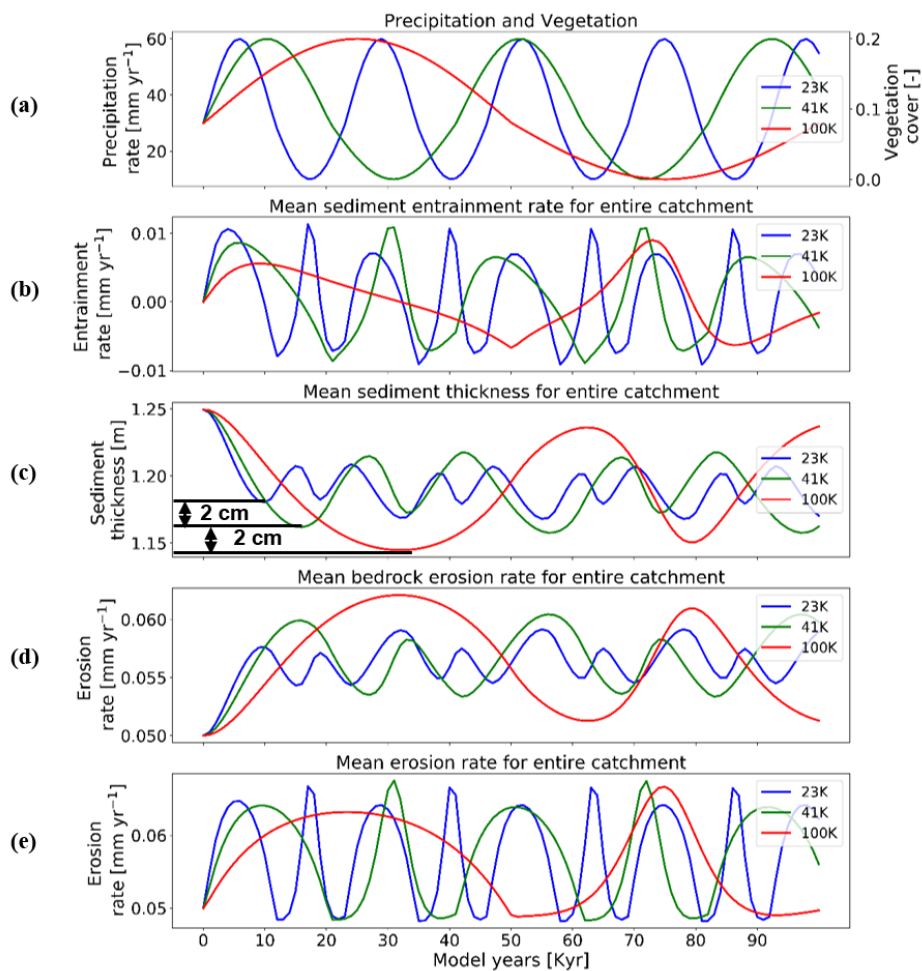
285 Mean catchment sediment thicknesses in the 10% vegetation cover simulation show a modest response and vary between 1.16
286 m – 1.24 m (Fig. 7c), and with a time lag of ~2.5 kyr between the peak in precipitation/vegetation and minimum sediment
287 thickness. This lag is also observed in the case of the 70% vegetation cover simulation, but with a higher amplitude of change
288 in sediment thickness (e.g. 2 m – 2.22 m, Fig. 7c). A similar trend in time lags between the peaks in climate/vegetation and
289 bedrock erosion (Fig. 6d) is also present. These observations for variations in sediment thickness again represent the combined
290 effects of the results discussed in section 3.1 and 3.2 (Figs. 5c, 6c).

291 The amplitude of change in bedrock erosion is between 0.05 mm yr^{-1} – 0.06 mm yr^{-1} for 10% veg., and 0.05 mm yr^{-1} – 0.08
292 mm yr^{-1} for 70% veg. (Fig. 7d). The bedrock erosion response for both simulations represents a composite of the effects shown
293 in the previous two scenarios (sections 3.1, 3.2). Here the increase in time lag in the maximum in erosion rates (most notable
294 for the 70% vegetation cover simulation) resembles the effect of a large increase in precipitation rates (compared Fig. 5d) for
295 the first part of the cycle. Whereas, the second peak in bedrock erosion visible in the 10% vegetation cover scenario more
296 closely resembles the effects shown in Fig 6d when the vegetation cover goes to 0% and the landscape is increasingly sensitive
297 to erosion with whatever runoff (albeit little) is available.

298 Finally, the mean catchment erosion rates (Fig. 7e) again show the combined effects of the sediment entrainment rate and
299 bedrock erosion histories previously discussed (Figs. 7b, d). In the simulation with 70% initial vegetation cover, the mean
300 catchment erosion rates follow the pattern of change in precipitation rates (e.g. ranging from 0.04 mm yr^{-1} to 0.1 mm yr^{-1} , Fig.
301 7e, see also Fig. 5e). A similar trend is present in the first half of the cycle in the simulation with 10% vegetation cover, but
302 with much lower magnitudes (i.e., 0.05 mm yr^{-1} to 0.06 mm yr^{-1} , Fig. 7e). However, during the second half of the cycle, the
303 erosion rates increase up to $\sim 0.06 \text{ mm yr}^{-1}$ and have a second peak at ~17-18 kyr for the 10% vegetation simulation when the
304 vegetation cover is a 0%. The previous result is however in contradiction to the detachment-limited results shown in Fig 17 of
305 Schmid et al. (2018), who found that erosion rates decreased to 0 mm yr^{-1} for the period of no vegetation cover and minimum
306 precipitation rate of ($\sim 10 \text{ mm yr}^{-1}$). This contradiction is related to the increase in sediment entrainment at this time (Fig. 7b)
307 which heavily influences the mean erosion. The detachment-limited approach of Schmid et al. (2018) could not account for
308 this, and will be discussed in detail in section 4.2. To summarize, as discussed previously the locations of the maximums and
309 minimums in the mean erosion rate and the shape of the curves (Fig. 7e) can be linked to different times in the climate and
310 vegetation history when either the effects of variable precipitation rate or vegetation cover dominate the mean catchment
311 erosional response.

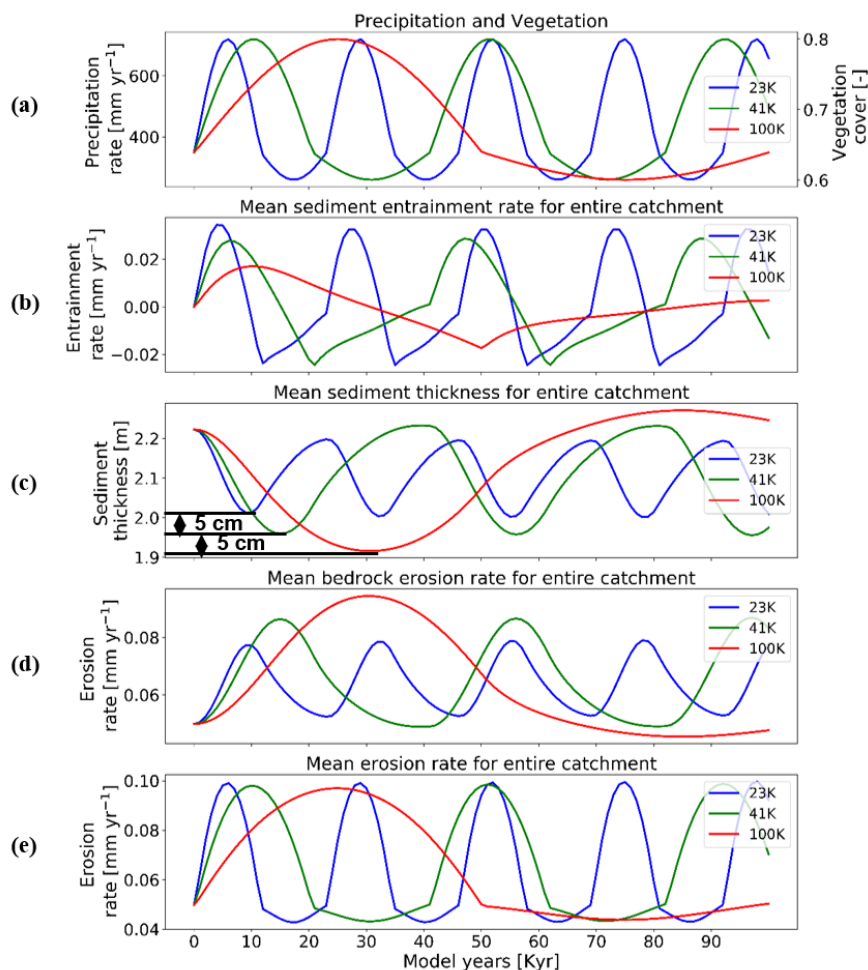
312 3.4 Influence of the periodicity of precipitation/vegetation variations on erosion and sedimentation (Scenario 4)

313 Here we show the influence of different periodicities (23, 41, and 100 kyr) in precipitation and vegetation change on catchment
314 erosion and sedimentation for the cases of a 10% mean vegetation cover (Fig. 8) and 70% vegetation cover (Fig. 9). We find
315 higher variations in mean sediment entrainment rates (Fig. 8b, 9b) for both the 10% and 70% vegetation cover simulations for
316 the shorter periodicities (23 and 41 kyr). However, the phase lag in the peaks of sediment entrainment and precipitation rates
317 was higher for longer periodicities (e.g. ~9%, ~16.2%, ~19% in 23 kyr, 43 kyr, and 100 kyr respectively) for the 10% vegetation
318 cover case (Fig. 8b). These phase lags are however, dampened in the highly vegetated landscapes (70%) at longer periods (i.e.,
319 ~9%, ~9.5%, ~14% in 23 kyr, 43 kyr, and 100 kyr respectively, Fig. 9b). In a landscape with 10% vegetation cover, the
320 simulation with longer periodicity (100 kyr) shows higher variations in mean catchment sediment thickness (e.g. 1.14 cm -
321 1.25 cm, Fig. 8c). This is mimicked in the landscape with 70% vegetation cover, with the range of sediment thickness between
322 1.95 cm – 2.27 cm (Fig. 9c). A similar trend with higher amplitude of change is also observed for bedrock erosion rates in the
323 sparsely vegetated landscape (10%) with values ranging from 0.05 mm a^{-1} to 0.062 mm yr^{-1} (Fig. 8d) for longer periodicity
324 (100 kyr). The same pattern is observed in highly vegetated landscapes (70%), with the values of bedrock erosion rates ranging
325 from 0.045 mm yr^{-1} to 0.094 mm yr^{-1} (Fig. 9d) for the longer periodicity (100 kyr).



326

327 **Figure 8: Temporal evolution of catchment averaged predictions for scenario 4 described in the text (section 3.4). Graphical**
 328 **representation of mean catchment sedimentation and erosion to (a) different periodicities of coupled oscillations in precipitation**
 329 **[mm yr⁻¹] and vegetation cover [-] in terms of (b) sediment thickness [m], (c) bedrock erosion [mm yr⁻¹], (d) sediment entrainment**
 330 **[mm yr⁻¹], (e) net erosion rates [mm yr⁻¹] for entire catchment. The rate of rock uplift is kept constant as 0.5 mm yr⁻¹. The simulations**
 331 **represent 10% initial vegetation cover.**



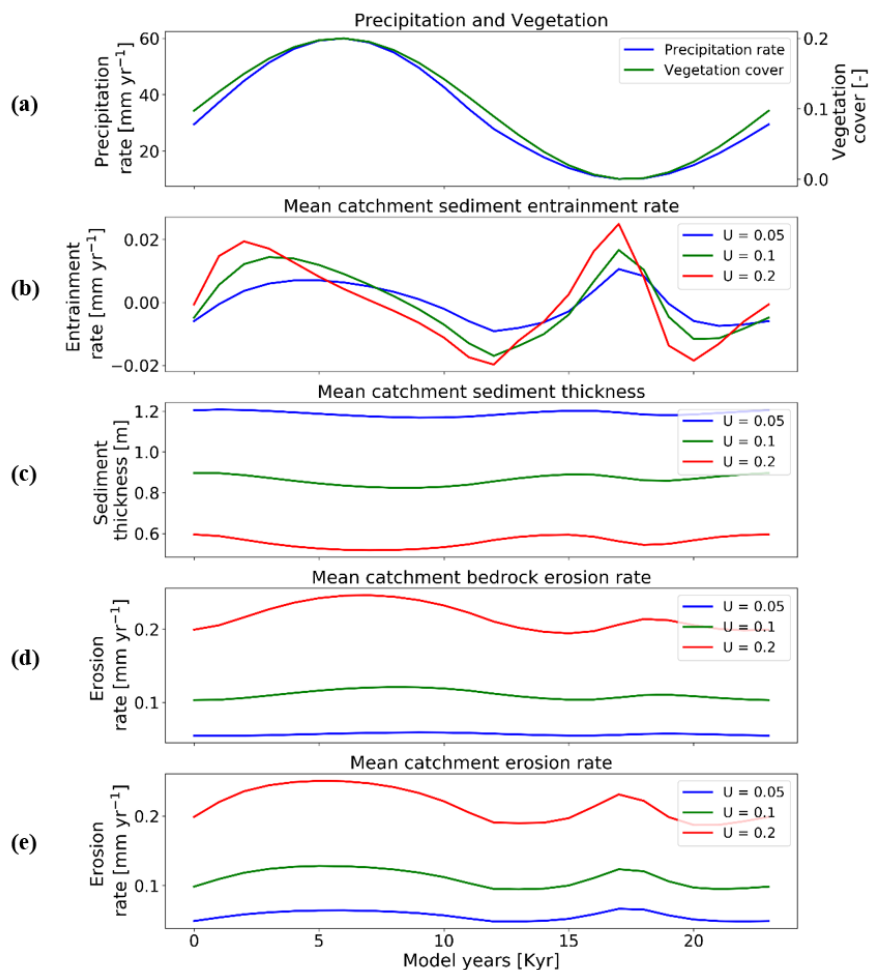
332

333 **Figure 9: Temporal evolution of catchment averaged predictions for scenario 4 described in the text (section 3.4). Graphical**
334 **representation of mean catchment sedimentation and erosion to (a) different periodicities of coupled oscillations in precipitation**
335 **[mm yr⁻¹] and vegetation cover [-] in terms of (b) sediment thickness [m], (c) bedrock erosion [mm yr⁻¹], (d) sediment entrainment**
336 **[mm yr⁻¹], (e) net erosion rates [mm yr⁻¹] for entire catchment. The rate of rock uplift is kept constant as 0.5 mm yr⁻¹. The simulations**
337 **represent 70% initial vegetation cover.**

338 Overall variations in mean catchment erosion rates (Fig. 8e, 9e) were not observed to be significant ($< 0.0001 \text{ mm yr}^{-1}$) as the
339 period of precipitation and vegetation change increases.

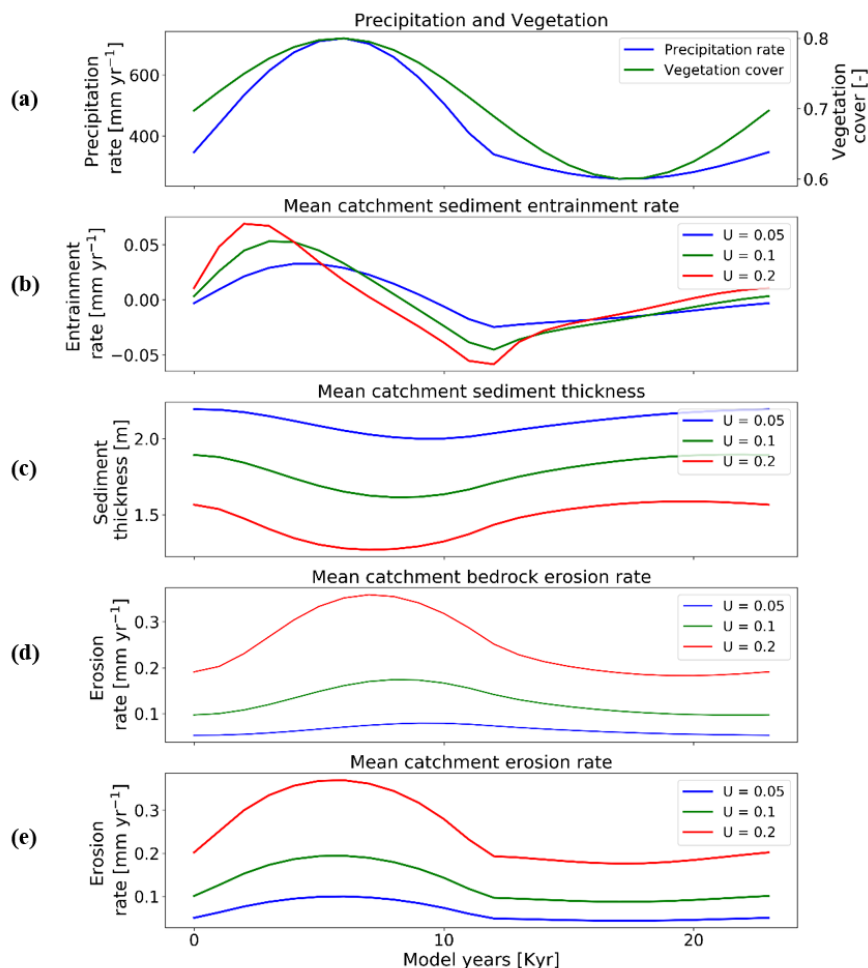
340 3.5 Influence of rock uplift rate and oscillating precipitation/vegetation on erosion sedimentation (Scenario 5)

341 Here we investigate the response of mean catchment erosion and sedimentation for different rates of rock uplift (i.e., 0.05 mm
342 a^{-1} , 0.1 mm a^{-1} , 0.2 mmyr^{-1}) for the 10% vegetation cover (Fig. 10) and 70% vegetation cover (Fig. 11) scenarios. To simplify
343 the presentation and comparison of results, the periodicity of precipitation and vegetation change is kept the same as section
344 3.3 (i.e., 23 kyr). In general, the results discussed below demonstrate that the transient catchment response to coupled
345 oscillations in precipitation rate and vegetation cover are similar in shape regardless of the rock uplift rate. The magnitude of
346 change in mean catchment erosion associated with precipitation and vegetation changes increases with increasing uplift rate,
347 despite an identical amount of vegetation and precipitation change imposed (Figs. 10a, 11a) on each rock uplift rate simulation.



348

349 **Figure 10: Temporal evolution of catchment averaged predictions for scenario 5 described in the text (section 3.5). Graphical**
 350 **representation of mean catchment sedimentation and erosion with different rates of rock uplift [mm a⁻¹] to (a) coupled oscillations**
 351 **in precipitation [mm yr⁻¹] and vegetation cover [-] in terms of (b) sediment thickness [m], (c) bedrock erosion [mm yr⁻¹], (d) sediment**
 352 **entrainment [mm yr⁻¹], (e) net erosion rates [mm yr⁻¹] for entire catchment. The periodicity of climate and vegetation oscillations is**
 353 **23 kyr. The simulations represent 10% initial vegetation cover.**



354

355 **Figure 11: Temporal evolution of catchment averaged predictions for scenario 5 described in the text (section 3.5). Graphical**
 356 **representation of mean catchment sedimentation and erosion with different rates of rock uplift [mm a⁻¹] to (a) coupled oscillations**
 357 **in precipitation [mm yr⁻¹] and vegetation cover [-] in terms of (b) sediment thickness [-], (c) bedrock erosion [mm yr⁻¹], (d) sediment**
 358 **entrainment [mm yr⁻¹], (e) net erosion rates [mm yr⁻¹] for entire catchment. The periodicity of climate and vegetation oscillations is**
 359 **23 kyr. The simulations represent 70% initial vegetation cover.**

360 In more detail, the temporal pattern of changes in sediment entrainment rates (Fig. 10b, 11b) is similar for all uplift rates
 361 considered, but the amplitude of change increases as the uplift rate increases. In addition, the phase lag between the peaks in
 362 sediment entrainment rates and precipitation rates in the 10% vegetation simulation (Fig. 10d) varies with the rock uplift rate.
 363 The sediment entrainment rates are higher for lower rock uplift rates (e.g. ~ -4 kyr, -2.5 kyr, -2 kyr) before the maximum in
 364 precipitation for rock uplift rates of 0.05 mm a⁻¹, 0.1 mm a⁻¹, and 0.2 mm a⁻¹, respectively (Fig. 10b). However, the phase lags
 365 are overall shorter in highly vegetated landscapes (70%) (e.g. ~ -3 kyr, -2 kyr, -1 kyr) before the maximum in precipitation for
 366 rock uplift rates of 0.05 mm a⁻¹, 0.1 mm a⁻¹, and 0.2 mm a⁻¹ respectively (Fig. 11b).

367 For the landscape with 10% vegetation cover, the simulation with the highest rates of rock uplift (0.02 mm a⁻¹) showed lower
 368 mean catchment sediment thickness (e.g. ~0.5 m – ~0.6 m, Fig. 10c). In contrast, the slowest rock uplift simulation (0.05 mm
 369 a⁻¹) had thicker sediment thickness of ~1.16 m – ~1.24 m, (Fig. 10c). The same pattern was observed in the catchment with
 370 70% vegetation cover, where the higher sediment thicknesses occur for the lower rates of rock uplift (e.g. ~2 m - ~2.2 m, Fig.
 371 11c). These results for sediment thickness variations reflect that higher rock uplift rates result in steeper slopes (not shown)



372 and higher mean catchment erosion rates (Figs. 10e, 11e) such that regolith production rates are outpaced by erosion and
373 therefore result in thinner sediment thicknesses. This result is akin to the observational results of Heimsath et al. (1997).
374 Temporal variations in bedrock and mean catchment erosion rates are similar to those described in section 3.3 (Fig. 7) for the
375 sparsely and more heavily vegetated conditions. The primary difference is that at high rock uplift rates the amplitude of
376 bedrock or mean catchment erosion increases (Figs. 10d,e; 11d,e). To summarize, these results highlight that regardless of the
377 rock uplift rate, similar temporal changes are observed in sediment entrainment or thickness, and in bedrock and catchment
378 erosion for oscillating precipitation rates and vegetation cover. However, the amplitude of change (or absolute change) in
379 entrainment and erosion rates increases with increases in rock uplift rate. This will be discussed in detail in section 4.4.

380 **4 Discussion**

381 In this section, we synthesize the results from previous section (scenarios 1-5) in detail. We further look deeply into the
382 effects of coupled climate and vegetation oscillations (Scenario 3) on the occurrence of erosion and sedimentation on spatial
383 scale.

384 **4.1 Differences in effects between oscillating vegetation or precipitation**

385 Here the sensitivity of erosion and sedimentation to variable precipitation and/or vegetation cover is analysed. In the scenario
386 with oscillating precipitation and constant vegetation cover, sparsely vegetated landscapes (10%) are eroding slowly during
387 periods of lower precipitation. This might be attributed to the dependency of the bedrock erosion and sediment entrainment on
388 the amount of water available through precipitation, which in turn affects the erosion rates. The net erosion in this scenario is
389 dominated by bedrock erosion with a significant contribution from sediment entrainment.

390 Similarly, in a scenario with constant precipitation and variable vegetation cover, sparsely vegetated landscapes (10%) are
391 observed to be much more sensitive in terms of erosion rates during periods of no vegetation cover. The amplitude of erosional
392 change was ten times higher than that of densely vegetated landscapes. The net erosion in sparsely vegetated landscapes is
393 dominated equally by bedrock erosion (Fig. 6d) and sediment entrainment, due to the higher availability of bare soil. This
394 justifies the argument of a higher sensitivity of sparsely vegetated landscapes to erosion and sedimentation. Also, a small
395 change in vegetation cover in densely vegetated landscapes would not result in significant differences in erosional processes.
396 In general, mean catchment sediment thickness is observed to be inversely proportional to precipitation, owing to higher
397 discharge rates. This in turn translates to a higher sediment flux during wetter periods. The influence of oscillating precipitation
398 and constant vegetation cover on sediment thickness is slightly higher in simulations with sparse vegetation cover. In
399 simulations with constant precipitation and oscillating vegetation cover, the sensitivity of sediment thickness is much higher
400 in landscapes with sparse vegetation. This can be attributed to an absence of vegetation cover when it is minimum. A decreased
401 impact of oscillating vegetation cover on sediment thickness occurs in landscapes with denser vegetation cover and
402 demonstrates that surface processes in these settings are not highly dependent on changes in vegetation density. This has been
403 explained by Huxman et al. (2004), who found that vegetation cover responds as sensitive to MAP in wet and dry systems
404 during dry years.

405 **4.2 Synthesis of coupled oscillations of precipitation and vegetation cover simulations**

406 The sensitivity of erosion and sedimentation to coupled oscillations in precipitation and vegetation cover (scenario 3, section
407 3.3) indicates that mean catchment erosion rates (Fig. 7e) are correlated with precipitation for densely vegetated landscapes
408 (70%). This is owed to the dominating effect of mean annual precipitation changes (from 26 cm yr⁻¹ to 72 cm yr⁻¹) on erosion
409 over vegetation cover change (from 60% to 80%, Fig. 7a) in these landscapes. This can be attributed to the higher amplitude
410 of precipitation oscillations in these simulations required to change vegetation cover by +/-10% (Fig. 2b). In the case of a



411 sparsely vegetated landscape (10%), mean erosion rates (Fig. 7e) are also correlated to precipitation, but only for the first half
412 of the cycle when vegetation cover is present. However, mean erosion rates increase rapidly in the second half of the cycle
413 when MAP decreases (from 60 mm yr⁻¹ to 10 mm yr⁻¹, Fig. 7a) and vegetation cover magnitudes decrease (from 20% to 0%,
414 Fig. 7a). This inverse correlation between precipitation and erosion can be attributed to increasing susceptibility of the surface
415 to sediment entrainment as vegetation cover decreases to bare soil, even with very low precipitation rates.
416 Thus, the temporal evolution of mean erosion rates between the heavily (70%) and sparsely (10%) vegetated landscapes varies
417 depending on the initial vegetation state of the catchment. As a result, correlated and anti-correlated relationships between
418 precipitation, vegetation cover, and erosion are predicted and are the result of precipitation or vegetation exerting a dominant
419 or subsidiary influence on catchment erosion at different times in the catchment history and for different catchment
420 precipitation and vegetation cover conditions. This prediction is consistent with observed correlations of vegetation cover and
421 catchment average erosion rates recently documented along the western Andean margin by Starke et al. (2020).

422 4.3 Differences between the periodicities of climate and vegetation cover oscillations

423 The periodicity of change in climate will mainly affect vegetation via the lag-time it takes for the vegetation to respond i.e., if
424 the vegetation structure does not change (e.g., grasslands or forests), then grasslands are very flexible (Bellard et al., 2012;
425 Kelly and Goulden, 2008; Smith et al., 2017). Grasslands can plastically respond from year to year while forests may die off
426 and be replaced by grasslands when it becomes drier and vice-versa. This change in vegetation type might lead to the
427 fluctuations in sedimentation and erosion rates due to periodicity of change in climate and vegetation cover.

428 4.4 The effect of rock uplift rate on signals of varying precipitation and vegetation cover

429 No difference in erosion rates was identified between the two different vegetation/precipitation simulations for a given uplift
430 rate when the erosion rate is averaged over the full period of vegetation/precipitation change. In a steady state landscape,
431 erosion rates are equal to the rock uplift rates according to the law of continuity of mass (Tucker et al., 2001). This means that
432 steady state landscapes experience higher erosion rates with higher uplift rates. However, the mean catchment erosion rates
433 shown in Fig. 10e, 11e show temporal variations in the erosion rate driven by oscillations in the precipitation rate and
434 vegetation. When average erosion rates are calculated over a complete cycle of the oscillation, the mean erosion rate equals
435 the rock uplift rate. This result indicates that any climate or vegetation driven changes in erosion will not be evident when
436 observed over too long a period time, but might introduce shorter-term transients (high or low) depending on the
437 climate/vegetation cycle of change. This finding is significant for observational studies seeking to measure the predictions
438 shown in this study. More specifically, thermochronometer dating approaches used to quantify denudation rates over million-
439 year timescales will be hard pressed to measure any signal of how climate or vegetation change on Milankovitch timescales
440 influence denudation. Rather, the rate of tectonic rock uplift or exhumation (in the case of erosion rates equalling the rock
441 uplift rate) will be measured. In contrast, observational techniques sensitive to decadal (e.g. sediment fluxes) or millennial
442 (e.g. cosmogenic radio nuclides measured from river terraces) can be sensitive to timescales less than the period of oscillation
443 and are more like to record transient catchment erosion rates influenced by variations in precipitation or vegetation cover.

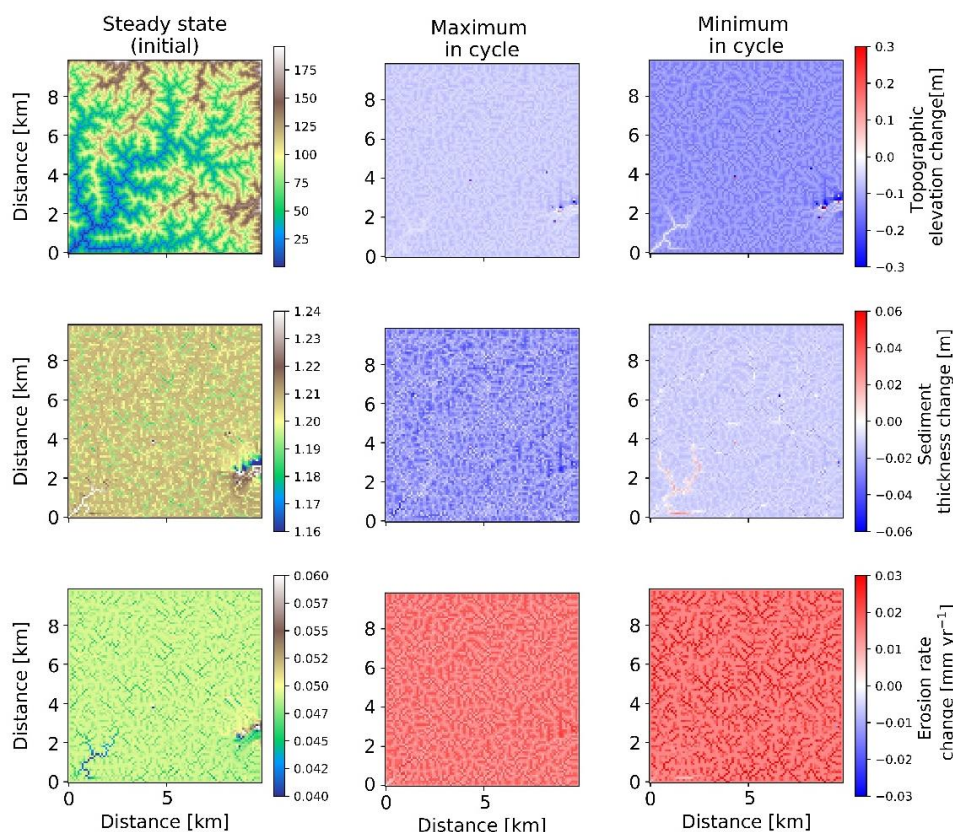
444 The vegetation and precipitation driven transients in mean catchment erosion rates predicted by this study were large enough
445 to be measured by some observational techniques. For example, in sparsely vegetated landscapes the half amplitude of change
446 in erosion rates (from steady-state values) slightly decreases as the uplift rate increases. A higher magnitude of change in
447 transient erosion rates (from steady-state values) is found in densely vegetated landscapes and is again slightly decreasing as
448 the uplift rate increases. Previous work by Schaller and Ehlers (2006) investigated the ability of denudation rates calculated
449 from cosmogenic radionuclides measured in a sequence of fluvial terraces to record periodic (Milankovitch timescale)
450 variations in denudation rates. The magnitude of change in predicted transient erosion rates described above is above the
451 detection limit reported by Schaller and Ehlers (2006), particularly when the mean catchment denudation rate is ~0.1 mm yr⁻¹



452 or higher. Thus, the predictions suggested in this study are testable in field-based studies, and other methods such as basin
453 sedimentation rate histories (e.g. determined from magneto-stratigraphy or other methods) also hold potential.

454 4.5 Spatial changes in where erosion and sedimentation changes occur

455 In the previous sections our analysis focused on the spatially averaged response of the catchment in terms of changes in
456 sedimentation and erosion. Here, we discuss the same model results as previously presented for but show two examples (for
457 two different vegetation covers) of the spatial variations of erosion and sediment thickness within the catchments. This
458 provides a basis for understanding where in the catchment changes are occurring.



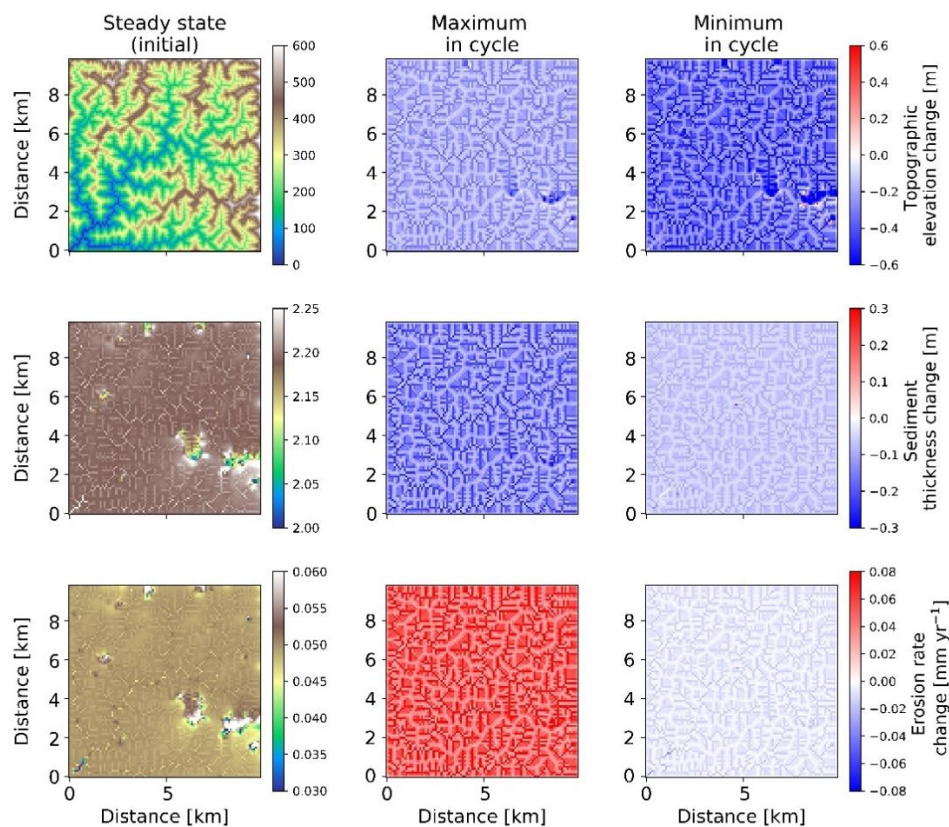
459

460 **Figure 12:** Two-dimensional map-view representation of changes in topographic elevations [m] (1st row), sediment thickness [m] (2nd
461 row), and erosion rates [mm yr⁻¹] (3rd row). These changes are represented with respect to steady state conditions (1st column), for
462 maximum (2nd column) and minimum (3rd column) values of precipitation and vegetation in an oscillation cycle. The simulations
463 represent 10% initial vegetation cover.

464 Spatial variations in the pattern of erosion and sedimentation in the simulations with 23 kyr coupled precipitation and
465 vegetation oscillations, and a rock uplift rate of 0.05 mm a⁻¹, are shown in the topographic elevation, sediment thickness, and
466 erosion rate changes for both the maximum and minimum in precipitation and vegetation cover. In the simulations with sparse
467 vegetation cover (10%) (Fig. 12) at the maximum in precipitation and vegetation cover, erosion rate changes from steady state
468 are ~0.03 mm yr⁻¹ in valleys and ~0.01 mm yr⁻¹ on hillslopes. At the minimum in precipitation and vegetation cover, erosion
469 rate changes from steady state are higher in valleys hillslopes. This may be attributed to an absence of vegetation during this
470 period, where the surface (bedrock or sediment) is readily available for erosion even with lower precipitation rates. The
471 sediment thickness is observed to be slightly higher in the streambeds and valleys for streams with larger accumulation area.
472 However, the smaller streams have lower sediment thickness compared to connected hillslopes. For example, higher sediment



473 thickness (~1.24 m) is observed near the catchment outlet in the lower-left corner of the domain. At the maximum in
474 precipitation and vegetation cover cycle, the landscape experiences a slightly higher contrast in sediment thickness compared
475 to the steady-state condition, whereby a net lowering of the sediment layer is observed of approximately 2 cm to 5 cm on the
476 hillslopes and ~6 cm near the catchment outlet. This can be attributed to higher sediment fluxes during this period. At the
477 minimum in the precipitation and vegetation cover cycle, the landscape experiences a slight difference from the steady state
478 sediment thickness (~2 cm lowering) except for deposition in higher order streams (up to ~2 cm) near the catchment outlet.



479

480 **Figure 13. Two-dimensional map-view representation of changes in topographic elevations [m] (1st row), sediment thickness [m] (2nd**
481 **row), and erosion rates [mm yr⁻¹] (3rd row). These changes are represented with respect to steady state conditions (1st column), for**
482 **maximum (2nd column) and minimum (3rd column) values of precipitation and vegetation in an oscillation cycle. The simulations**
483 **represent 70% initial vegetation cover.**

484 In the simulations with dense vegetation cover (70%) (Fig. 13), erosion rate changes from steady state conditions are higher
485 during the maximum in the precipitation and vegetation cover cycle with higher magnitudes (~0.08 mm yr⁻¹ in valleys and up
486 to ~0.02 mm yr⁻¹ on hillslopes and ridges) due to the higher precipitation rates. At minimum precipitation and vegetation cover
487 magnitudes (P = 26 cm; V = 60%), erosion rate changes are reduced (up to -0.03 mm yr⁻¹ in valleys and (up to -0.01 mm yr⁻¹)
488 on hillslopes in comparison to the erosion rates at steady state. Sediment thickness is observed to be relatively higher in the
489 streambeds and valleys (~2.25 m) than the hillslopes. It is contrastingly higher in the lowlands than the areas at higher
490 elevations. At maximum precipitation and vegetation cover (maximum in the cycle) sediment thickness is ~10 cm lower on
491 hillslopes and up to ~30 cm lower in valleys. The same trend with lower amplitude is evident for the minimum in the
492 precipitation and vegetation cover cycle. This implies that at higher vegetation cover, sediment thickness is significantly
493 reduced as a result of higher sediment flux during the peak in precipitation rates. This in turn signifies the dominance of
494 precipitation changes over vegetation cover change in highly vegetated landscapes.



495 **4.6 Comparison to previous studies**

496 Results presented in this study document a higher sensitivity of catchment erosion and sedimentation of sparsely vegetation
497 landscapes (10%) to changes in vegetation cover, whereas densely vegetated (70%) landscapes are more responsive to changes
498 in precipitation than vegetation changes. This confirms the broad findings of Schmid et al. (2018), which suggested
499 vulnerability of erosion rates in sparsely vegetated landscapes to the changes in vegetation cover and that for densely vegetated
500 landscapes to the changes in MAP. However, there are differences between Schmid et al. (2018) and this study, particularly
501 for the temporal changes in erosion rates we observe for the sparse vegetation cover (10%) scenario with coupled
502 precipitation/vegetation cover oscillations. More specifically, previous results from the detachment limited model shown in
503 Fig. 17 of Schmid et al. (2018) show that catchment erosion rates in sparsely vegetated landscapes decrease as the precipitation
504 and vegetation cover increases in the first part of a cycle. In the second part of the cycle when precipitation and vegetation
505 decrease to their minimum Schmid et al. (2018) predict erosion rates are ~ 0 mm yr⁻¹. However, in the coupled detachment-
506 transport fluvial erosion model presented here (SPACE), we observe a different behavior and erosion rates slightly increase as
507 precipitation and vegetation cover increase (from 0.05 mm yr⁻¹ to 0.065 mm yr⁻¹, Fig. 7(e)), rather than decrease. This
508 difference is due to higher sediment entrainment rates we predict during the period of no vegetation and low precipitation (10
509 mm yr⁻¹), which is a result of higher vulnerability of bare soil to erosion, even with very low precipitation rates. Therefore, the
510 application of a detachment limited, vs. coupled detachment-transport limited modelling approach has bearing on the predicted
511 response, and when comparing results to natural systems care should be taken in which approach is used.

512 Previous geochemistry related observational studies from the Chilean Coastal Cordillera (EarthShape study areas) are also
513 available for comparison to this study. For example, the steady-state sediment thickness in our simulations for 10% and 70%
514 initial vegetation cover are predicted to be higher than the field observations reported by Schaller et al. (2018) and Oeser et al.
515 (2018), who reported a ~ 20 cm and ~ 60 cm depth of mobile sediment layers on hillslopes in the Pan de Azucar and La Campana
516 study areas, respectively. However, the trend in our results (higher sediment thickness for densely vegetated (70%) landscapes)
517 follows the findings of Oeser et al. (2018) who document that sediment depths increase with increasing mean annual
518 precipitation and vegetation in Chilean Coastal Cordillera. The explanation for the discrepancies between the observed and
519 predicted sediment thickness is unclear to us, but may highlight the need for future improvements in soil production functions
520 used in landscape evolution models.

521 In addition, previous field studies (Oeser et al., 2018; Owen et al., 2011; Schaller et al., 2018) applied cosmogenic nuclides to
522 estimate the denudation and soil production rates in the Chilean Coastal Cordillera. They suggest an increase in soil production
523 rates from arid zones in the north to wet tropical zones in the south of the Chilean Coastal Cordillera. These findings are
524 consistent with the predicted increase in sediment depths (e.g. 1.24 m for $V = 10\%$ and 2.22 m for $V = 70\%$, Fig. 7(b)) in our
525 study. Finally, the effects of rock uplift and precipitation rates on topography and erosion rates, as documented by Bonnet and
526 Crave (2003) and Lague et al. (2003) show a linear relationship between mean topographic elevation and rock uplift rate for
527 steady-state conditions. We find a similar relationship from our model predictions (Fig. 10a).

528 **4.7 Model limitations**

529 The model setup used in this study was intended to quantify the sensitivity of hillslope and fluvial erosion, and sediment
530 transport and depositional processes for different climates with variations in precipitation rates and vegetation cover over
531 Milankovitch time scales. This study was designed as an incremental step forward from previous modelling studies (Collins
532 et al., 2004; Guzman, 2019; Istanbuluoglu, 2005; Istanbuluoglu and Bras, 2006; Schmid et al., 2018).

533 There are several simplifying assumptions made in our modelling approach that warrant discussion and potential investigation
534 in future studies. For example, this study assumed uniform vegetation cover and lithology for the entire catchment. The
535 assumption of uniform vegetation cover in the catchment is likely reasonable given that relatively small (10×10 km²) size of
536 catchments investigated and the modest topographic relief produced (between ~ 75 -600m, Fig. 10a). Although temperature and



537 precipitation (and therefore vegetation cover) can vary with elevation, the generally low relief of the catchments in this study
538 do not make this a major concern. Due to the long (geologic) timescales considered in this study and computational
539 considerations, mean annual precipitation rates were applied and stochastic distributions of precipitation could not be
540 considered. While our approach is common for landscape evaluation modelling studies conducted on geologic timescales, we
541 recognize that in some settings (such as the arid region of this study, Fig. 1) precipitation events are rare, stochastic in nature,
542 and might have an influence in the results presented here. This is a caveat that warrants future investigation.

543 The vegetation-erosion parameterization considered in this study follows from that of Istanbuluoglu and Bras (2006) and
544 Schmid et al. (2018). In this parameterization only, the total vegetation cover of the catchment is considered, rather than the
545 distribution of vegetation cover by individual plant functional types (e.g. grass, shrubs, trees) that would have different
546 Manning's coefficients associated with them. The 'total vegetation cover' approach used in our (and previous) work is a
547 reasonable starting point for understanding landscape evolution over large spatial and temporal scales because: a) more detailed
548 observations about the changes in the distribution of plant functions type over Milankovitch timescales is not available and
549 would be poorly constrained, and b) empirical relationships between total vegetation cover and precipitation are available and
550 easily implemented (e.g. Fig. 2b). However, future work should focus on exploring how the temporal and spatial distribution
551 of different plant functional types during changing climate impacts catchment erosion given that recent work (Mishra et al.,
552 2019; Starke et al., 2020) has identified this as important. This limitation can be handled in future studies with the full coupling
553 of a dynamic vegetation models, such as LPJ-GUESS (Smith et al., 2014; Werner et al., 2018) to a landscape evolution model
554 for the explicit treatment of how different vegetation types change temporally and spatially within a catchment and influence
555 catchment erosion. Lastly, the time-scale for the current study was based on Milankovitch cycles, to address the effects of
556 periodicity on erosion and sedimentation. However, the effects of seasonal (sub annual) variations in precipitation/vegetation
557 also warrants future investigation to identify if seasonal variations in vegetation cover and precipitation influence catchment
558 erosion.

559 Finally, the results of this study rely upon the vegetation-erosion parameterizations described in section 2 and the appendix
560 (see also Fig. 3). While there is an observational basis for these relationships (see section 1.1, 1.2 in Appendix) there are,
561 frankly, a sparse number of field studies available robustly constraining how different vegetation types and amounts influence
562 hillslope and surface water erosional processes. Thus, we consider the erosional parameterizations used here as hypotheses
563 (rather than robust geomorphic transport laws) that warrant investigation in future field or flume studies.

564 **5 Summary and Conclusions**

565 The objective of this study were to test the hypotheses that: (1) if vegetation cover and climate vary on Milankovitch timescales,
566 then any increases or decreases in catchment erosion will be large amplitude over longer (e.g. 100 kyr) rather than shorter (e.g.
567 21 kyr) periodicities due to the longer duration of any climate or vegetation change occurring at longer periodicities; and (2)
568 if increasing rates of tectonic uplift cause increases in catchment erosion rates, then any periodic variations in climate and
569 vegetation cover will be muted (lower amplitude) at higher uplift rates as the effect of rock uplift outweigh climate and
570 vegetation changes. The approach used here complements previous studies by using a coupled detachment-transport limited
571 model, and also investigates the degree to which transient effects of vegetation cover and precipitation are measurable in
572 observational studies. The main conclusions deduced from this study are:

- 573 i. The step-wise increase in complexity of the model simulations was essential for identifying temporal changes in
574 catchment erosion and sediment thickness. A non-linear response in erosion and sediment thickness to varying
575 precipitation and vegetation cover was observed and results were dependent on the initial vegetation and precipitation
576 state of the catchment. The sources of non-linearity stem from: a) a non-linear relationship between precipitation
577 changes required to cause +/-10% change in vegetation cover (Fig. 2); and b) exponential and power-law relationships



- 578 in the prescribed vegetation dependent hillslope and fluvial, respectively, geomorphic transport laws (Fig. 3, see also
579 Appendix).
- 580 ii. Analysis of results for covarying precipitation and vegetation cover indicate that erosion and sedimentation in densely
581 vegetated landscapes ($V = 70\%$) are more heavily influenced by changes in precipitation than changes in vegetation
582 cover. This is due to the higher amplitude of precipitation change needed to cause variations in vegetation cover in
583 densely vegetated settings (Fig. 5a, 7e).
- 584 iii. Analysis of results for covarying precipitation and vegetation cover indicate that erosion and sedimentation in sparsely
585 vegetated landscapes ($V = 10\%$) are more sensitive to variable vegetation cover with constant precipitation rates (Fig.
586 6, 7e), particular when precipitation rates decrease and vegetation cover approaches 0%.
- 587 iv. Concerning the first hypotheses: We found the effect of Milankovitch periodicity variations on the amplitude of
588 change in sediment thickness and bedrock erosion is more pronounced for longer climate and vegetation oscillations
589 (100 kyr) in both climate and vegetation settings. This finding confirms the hypothesis. Furthermore, periodicity
590 effects on erosion and sediment thickness are larger in densely (70%) vegetated landscapes than sparsely (10%)
591 vegetated landscapes, thereby indicating a sensitivity of the response to the biogeographic zone the changes are
592 imposed on.
- 593 v. With respect to our second hypothesis, all transient forcings in precipitation and vegetation cover explored in this
594 study resulted in variations in erosion and sediment thickness around the mean erosion rate, which is determined by
595 the rock uplift rate. As rock uplift rates increased from 0.05 mm a^{-1} to 0.2 mm a^{-1} , the effects of periodic changes in
596 precipitation and vegetation cover on erosion rates became more pronounced, and were between about 35% to 110%,
597 respectively, of the background rock uplift rate. This finding negates the hypothesis, and suggests that regardless of
598 the tectonic setting considered (within the range of rock uplift rates explored here) erosional transients from varying
599 precipitation and vegetation cover occur, but the detection of these changes requires measurement of erosion rates
600 integrating over short time scales such that the average (tectonically driven) mean erosion rate is not recovered.
- 601 vi. Finally, in comparison to previous studies, the 35% to 110% transient changes in erosion rate are at, or above, the
602 detection limit for measurement cosmogenic radionuclides in river sediments preserved in fluvial terraces, but would
603 be undetectable with bedrock thermochronometer dating techniques that average erosion rates over longer timescales.
604 The potential to measure vegetation related transient changes in erosion rates with cosmogenic nuclides is highest in
605 settings with higher rock uplift rates (e.g. 0.1 mm a^{-1} , 0.2 mm a^{-1}) and at longer (41 to 100 kyr) periodicities.

606 Appendix

607 1 Effect of vegetation and precipitation on hillslope and fluvial erosion

608 The approach followed in our study follows the law of continuity of mass (Tucker et al., 2001). It states that the rate of change
609 in topographic elevation (z) is defined as follows:

$$610 \frac{\partial z}{\partial t} = U - \frac{\partial z}{\partial t}(\text{fluvial}) + \frac{\partial z}{\partial t}(\text{hillslope}), \quad (1)$$

611 where, U is uplift rate [m yr^{-1}], t is time [yr]. The second and third terms on right-hand side refer to the rate change in
612 topographic elevation due to fluvial and hillslope processes respectively.

613 1.1 Vegetation dependent hillslope processes

614 The rate of change in topography due to hillslope diffusion (Fernandes and Dietrich, 1997; Martin, 2000) is defined as follows:



$$615 \quad \frac{\partial z}{\partial t}(\text{hillslope}) = \nabla q_s, \quad (2)$$

616 where q_s is sediment flux along the slope S . We applied slope and depth-dependent linear diffusion rule following the approach
 617 of Johnstone and Hilley (2014) such that:

$$618 \quad q_s = K_d S d_* \left(1 - e^{-\frac{H}{d_*}}\right), \quad (3)$$

619 where K_d is diffusion coefficient [$\text{m}^2 \text{yr}^{-1}$], d_* is sediment transport decay depth [m], and H denotes sediment thickness.
 620 The diffusion coefficient is defined as a function of vegetation cover present on hillslopes, which is estimated following the
 621 approach of Istanbuluoglu (2005), Dunne et al. (2010) and (Schmid et al., 2018) as follows:

$$622 \quad K_d = K_b e^{-(\alpha V)}, \quad (4)$$

623 where K_d is defined as a function of vegetation cover V , an exponential decay coefficient α , and linear diffusivity K_b for bare
 624 soil.

625 1.2 Vegetation dependent fluvial processes

626 The fluvial erosion is estimated for a two-layer topography (i.e., bedrock and sediment are treated explicitly) in the coupled
 627 detachment – transport limited model, SPACE 1.0 (Shobe et al., 2017). Bedrock erosion and sediment entrainment are
 628 calculated simultaneously in the model. Total fluvial erosion is defined as:

$$629 \quad \frac{\partial z}{\partial t}(\text{fluvial}) = \frac{\partial R}{\partial t} + \frac{\partial H}{\partial t}, \quad (5)$$

630 where, left-hand side denotes the total fluvial erosion rate. The first and second terms on right-hand side denote the bedrock
 631 erosion rate and sediment entrainment rate.

632 The rate of change of height of bedrock R per unit time [m yr^{-1}] is defined as:

$$633 \quad \frac{\partial R}{\partial t} = U - E_r, \quad (6)$$

634 where E_r [m yr^{-1}], is the volumetric erosion flux of bedrock per unit bed area.

635 The change in sediment thickness H [m] per unit time [yr] was calculated following Davy and Lague (2009) and Shobe et al.
 636 (2017). It is defined as a fraction net deposition rate and solid fraction sediments, as follows:

$$637 \quad \frac{\partial H}{\partial t} = \frac{D_s - E_s}{1 - \phi}, \quad (7)$$

638 where, D_s [m yr^{-1}] is the deposition flux of sediment, E_s [m yr^{-1}] is volumetric sediment entrainment flux per unit bed area, and
 639 ϕ is the sediment porosity.

640 Following the approach of Shobe et al. (2017), E_s and E_r given by:

$$641 \quad E_s = (K_s q^m S^n - \omega_{cs}) \left(1 - e^{-\frac{H}{H_*}}\right), \quad (8)$$

$$642 \quad E_r = (K_r q^m S^n - \omega_{cr}) e^{-H/H_*}, \quad (9)$$

643 where, K_s [m^{-1}] and K_r [m^{-1}] are the sediment erodibility and bedrock erodibility parameters respectively. The threshold stream
 644 power for sediment entrainment and bedrock erosion are denoted as ω_{cs} [m yr^{-1}] and ω_{cr} [m yr^{-1}] in above equations. Bedrock



645 roughness is denoted as H_s [m] and the term e^{-H/H_s} corresponds to the soil production from bedrock. With higher bedrock
646 roughness magnitudes, more sediment would be produced.

647 K_s and K_r were modified in the model using the approach of Istanbuluoğlu (2005) and Schmid et al. (2018) by introducing
648 the effect of Manning's roughness to quantify the effect of vegetation cover on bed shear stress:

$$649 \tau_v = \rho_w g (n_s + n_v)^{6/10} q^m S^n F_t, \quad (10)$$

650 where, ρ_w [kg m^{-3}] and g [m s^{-2}] are density of water and acceleration due to gravity respectively. Manning's numbers for bare
651 soil and vegetated surface are denoted as n_s and n_v . F_t represents shear stress partitioning ratio. Manning's number for
652 vegetation cover and F_t are calculated as follows:

$$653 n_v = n_{vr} \left(\frac{V}{V_r} \right)^w, \quad (11)$$

$$654 F_t = \left(\frac{n_s}{n_s + n_v} \right)^{\frac{3}{2}}, \quad (12)$$

655 where, n_{vr} is Manning's number for the reference vegetation. Here, V_r is reference vegetation cover ($V = 100\%$) and V is local
656 vegetation cover in a model cell, w is empirical scaling factor.

657 Through combining stream power equation (Gregory Tucker et al., 1999; Howard et al., 1994; Whipple and Tucker, 1999) and
658 above concept of the effect of vegetation on shear stress, we follow the approach of Schmid et al. (2018) to define new sediment
659 and bedrock erodibility parameters influenced by the surface vegetation cover on fluvial erosion, as follows:

$$660 K_{vs} = K_s \rho_w g (n_s + n_v)^{6/10} F_t, \quad (13)$$

$$661 K_{vr} = K_r \rho_w g (n_s + n_v)^{6/10} F_t, \quad (14)$$

662 where, K_{vs} [m^{-1}] and K_{vr} [m^{-1}] are modified sediment erodibility and bedrock erodibility respectively. These are influenced by
663 the effect of presence of fraction of vegetation cover V . Hence, K_s and K_r in Eq. (8) and Eq. (9) are replaced by K_{vs} and K_{vr} to
664 include an effect of vegetation cover on fluvial processes in the model. The trends of K_d , K_{vs} and K_{vr} are illustrated in Fig. 3.

665 **Code availability**

666 The code and data used in this study are freely available upon request.

667 **Author contributions**

668 MS, HS and TAE designed the initial model setup and simulation programs. HS and TAE conducted model modifications,
669 simulation runs and analysis. KT provided with an insight on qualitative assessment based on plant ecology in Chilean Study
670 areas. HS, TAE, and KT prepared the manuscript with contributions from all co-authors.

671 **Competing interests**

672 The authors declare that they have no competing interests.

673 **Acknowledgements**



674 H.S and T.A.E. acknowledge support from the Research Training Group 1829 Integrated Hydrosystem Modelling, funded by
675 the German Research Foundation (DFG). In addition, T.A.E, K.T. and M.S. acknowledge support from the German priority
676 research program (SPP-1803; grants EH329/14-1 and EH329/14-2 to T.A.E, and TI 338/14-1 and TI338/14-2 to K.T.). We
677 thank XXX, YYYY for constructive reviews.

678 **References**

679 Acosta, V. T., Schildgen, T. F., Clarke, B. A., Scherler, D., Bookhagen, B., Wittmann, H., von Blanckenburg, F. and Strecker,
680 M. R.: Effect of vegetation cover on millennial-scale landscape denudation rates in East Africa, *Lithosphere*, 7(4), 408–420,
681 <https://doi.org/10.1130/1402.1>, 2015.

682 Ahnert, F.: Some comments on the quantitative formulation of geomorphological processes in a theoretical model, *EARTH*
683 *SURFACE PROCESSES*, 2(2-3), 191–201, <https://doi.org/10.1002/esp.3290020211>, 1977.

684 Alonso, R. N., Bookhagen, B., Carrapa, B., Coutand, I., Haschke, M., Hilley, G. E., Schoenbohm, L., Sobel, E. R., Strecker,
685 M. R., Trauth, M. H. and Villanueva, A.: Tectonics, Climate, and Landscape Evolution of the Southern Central Andes: the
686 Argentine Puna Plateau and Adjacent Regions between 22 and 30°S, in *The Andes: Active Subduction Orogeny*, edited by O.
687 Oncken, G. Chong, G. Franz, P. Giese, H.-J. Götze, V. A. Ramos, M. R. Strecker, and P. Wigger, pp. 265–283, Springer Berlin
688 Heidelberg, Berlin, Heidelberg, , 2006.

689 Amundson, R., Heimsath, A., Owen, J., Yoo, K. and Dietrich, W. E.: Hillslope soils and vegetation, *Geomorphology*, 234,
690 122–132, <https://doi.org/10.1016/j.geomorph.2014.12.031>, 2015.

691 Ashkenazy, Y., Eisenman, I., Gildor, H. and Tziperman, E.: The Effect of Milankovitch Variations in Insolation on Equatorial
692 Seasonality, *Journal of Climate*, 23(23), 6133–6142, <https://doi.org/10.1175/2010JCLI3700.1>, 2010.

693 Avdievitch, N. N., Ehlers, T. A. and Glotzbach, C.: Slow Long-Term Exhumation of the West Central Andean Plate Boundary,
694 Chile, *Tectonics*, 37(7), 2243–2267, <https://doi.org/10.1029/2017TC004944>, 2018.

695 Bellard, C., Bertelsmeier, C., Leadley, P., Thuiller, W. and Courchamp, F.: Impacts of climate change on the future of
696 biodiversity, *Ecology Letters*, 15(4), 365–377, <https://doi.org/10.1111/j.1461-0248.2011.01736.x>, 2012.

697 Bonnet, S. and Crave, A.: Landscape response to climate change: Insights from experimental modeling and implications for
698 tectonic versus climatic uplift of topography, *Geology*, 31(2), 123–126, [https://doi.org/10.1130/0091-7613\(2003\)031<0123:Lrtcc>2.0.Co;2](https://doi.org/10.1130/0091-7613(2003)031<0123:Lrtcc>2.0.Co;2), 2003.

700 Braun, J., Voisin, C., Gurlan, A. T. and Chauvel, C.: Erosional response of an actively uplifting mountain belt to cyclic
701 rainfall variations, *Earth Surf. Dynam.*, 3(1), 1–14, <https://doi.org/10.5194/esurf-3-1-2015>, 2015.

702 Breckle, S.-W.: *Walter's Vegetation of the Earth*, 4th ed., Springer-Verlag Berlin Heidelberg, 2002.

703 Collins, D. B. G., Bras R. L. and Tucker G. E.: Modeling the effects of vegetation-erosion coupling on landscape evolution,
704 *Journal of Geophysical Research*, 109(F3), <https://doi.org/10.1029/2003jf000028>, 2004.

705 Dixon, J. L., Heimsath, A. M. and Amundson, R.: The critical role of climate and saprolite weathering in landscape evolution,
706 *Earth Surface Processes and Landforms*, 34(11), 1507–1521, <https://doi.org/10.1002/esp.1836>, 2009.

707 van Dongen, R., Scherler, D., Wittmann, H. and von Blanckenburg, F.: Cosmogenic ^{10}Be in river
708 sediment: where grain size matters and why, *Earth Surface Dynamics Discussions*, 1–31, <https://doi.org/10.5194/esurf-2018-83>, 2018.

710 Dosseto, A., Hesse, P. P., Maher, K., Fryirs, K. and Turner, S.: Climatic and vegetation control on sediment dynamics during
711 the last glacial cycle, *Geology*, 38(5), 395–398, <https://doi.org/10.1130/g30708.1>, 2010.

712 Gerten, D., Luo, Y., Le Maire, G., Parton, W. J., KEOUGH, C., WENG, E., BEIER, C., CIAIS, P., CRAMER, W., DUKES,
713 J. S., HANSON, P. J., KNAPP, A. A. K., LINDER, S., NEPSTAD, D., RUSTAD, L. and SOWERBY, A.: Modelled effects
714 of precipitation on ecosystem carbon and water dynamics in different climatic zones, *Global Change Biology*, 14(10), 2365–
715 2379, <https://doi.org/10.1111/j.1365-2486.2008.01651.x>, 2008.

716 Gilbert, G. K.: *Report on the geology of the Henry Mountains*, Report, Washington, D.C., 1877.



- 717 Guzman, C. D.: Hillslope sediment transport across climates and vegetative influences, *Geology*, 47(5), 495–496,
718 <https://doi.org/10.1130/focus052019.1>, 2019.
- 719 Hancock, G. S. and Anderson, R. S.: Numerical modeling of fluvial strath-terrace formation in response to oscillating climate,
720 *GSA Bulletin*, 114(9), 1131–1142, [https://doi.org/10.1130/0016-7606\(2002\)114<1131:NMOFST>2.0.CO;2](https://doi.org/10.1130/0016-7606(2002)114<1131:NMOFST>2.0.CO;2), 2002.
- 721 Heimsath, A. M., Dietrich, W. E., Nishiizumi, K. and Finkel, R. C.: The soil production function and landscape equilibrium,
722 *Nature*, 388(6640), 358–361, <https://doi.org/10.1038/41056>, 1997.
- 723 Herman, F., Rhodes, E. J., Braun, J. and Heiniger, L.: Uniform erosion rates and relief amplitude during glacial cycles in the
724 Southern Alps of New Zealand, as revealed from OSL-thermochronology, *Earth and Planetary Science Letters*, 297(1), 183–
725 189, <https://doi.org/10.1016/j.epsl.2010.06.019>, 2010.
- 726 Hopley, D. E. J., Adams, J. M., Nudurupati, S. S., Hutton, E. W. H., Gasparini, N. M., Istanbuluoglu, E. and Tucker, G. E.:
727 Creative computing with Landlab: an open-source toolkit for building, coupling, and exploring two-dimensional numerical
728 models of Earth-surface dynamics, *Earth Surface Dynamics*, 5(1), 21–46, <https://doi.org/10.5194/esurf-5-21-2017>, 2017.
- 729 Howard, A. D.: A detachment-limited model of drainage basin evolution, *Water Resources Research* 30(7), 2261–2285,
730 1994.
- 731 Huntley, B., Allen, J. R., Collingham, Y. C., Hickler, T., Lister, A. M., Singarayer, J., Stuart, A. J., Sykes, M. T. and Valdes,
732 P. J.: Millennial climatic fluctuations are key to the structure of last glacial ecosystems, *PLoS One*, 8(4), e61963,
733 <https://doi.org/10.1371/journal.pone.0061963>, 2013.
- 734 Huxman, T. E., Smith, M. D., Fay, P. A., Knapp, A. K., Shaw, M. R., Loik, M. E., Smith, S. D., Tissue, D. T., Zak, J. C.,
735 Weltzin, J. F., Pockman, W. T., Sala, O. E., Haddad, B. M., Harte, J., Koch, G. W., Schwinning, S., Small, E. E. and Williams,
736 D. G.: Convergence across biomes to a common rain-use efficiency, *Nature*, 429(6992), 651–654,
737 <https://doi.org/10.1038/nature02561>, 2004.
- 738 Hyun, S., Ahagon, N. and Yoon, H.-I.: Milankovitch cycles and paleoceanographic evolution within sediments from ODP
739 Sites 980 and 983 of the North Atlantic Ocean, *Geosciences Journal*, 9(3), 235, <https://doi.org/10.1007/BF02910583>, 2005.
- 740 Istanbuluoglu, E.: Vegetation-modulated landscape evolution: Effects of vegetation on landscape processes, drainage density,
741 and topography, *Journal of Geophysical Research*, 110(F2), <https://doi.org/10.1029/2004jf000249>, 2005.
- 742 Istanbuluoglu, E. and Bras, R. L.: On the dynamics of soil moisture, vegetation, and erosion: Implications of climate variability
743 and change, *Water Resources Research*, 42(6), <https://doi.org/10.1029/2005wr004113>, 2006.
- 744 Jeffery, M. L., Yanites, B. J., Poulsen, C. J. and Ehlers, T. A.: Vegetation-precipitation controls on Central Andean topography,
745 *Journal of Geophysical Research: Earth Surface*, 119(6), 1354–1375, <https://doi.org/10.1002/2013jf002919>, 2014.
- 746 Johnstone, S. A. and Hilley, G. E.: Lithologic control on the form of soil-mantled hillslopes, *Geology*, 43(1), 83–86,
747 <https://doi.org/10.1130/g36052.1>, 2014.
- 748 Kelly, A. E. and Goulden, M. L.: Rapid shifts in plant distribution with recent climate change, *Proc Natl Acad Sci USA*,
749 105(33), 11823, <https://doi.org/10.1073/pnas.0802891105>, 2008.
- 750 Kirby, E. and Whipple, K. X.: Expression of active tectonics in erosional landscapes, *Journal of Structural Geology*, 44, 54–
751 75, <https://doi.org/10.1016/j.jsg.2012.07.009>, 2012.
- 752 Kojima, S., Soto, I., Quiroz, M., Valencia, P. and Fernandez, I.: Geological and Geochemical Characteristics of the Intrusion-
753 Related Vein-Type Gold Deposits in the El Morado District, Coastal Cordillera, Northern Chile, *Resource Geology*, 67(2),
754 197–206, <https://doi.org/10.1111/rge.12129>, 2017.
- 755 Lague, D., Crave, A. and Davy, P.: Laboratory experiments simulating the geomorphic response to tectonic uplift, *Journal of*
756 *Geophysical Research: Solid Earth*, 108(B1), ETG 3-1-ETG 3-20, <https://doi.org/10.1029/2002jb001785>, 2003.
- 757 McPhillips, D., Bierman, P. R., Crocker, T. and Rood, D. H.: Landscape response to Pleistocene-Holocene precipitation change
758 in the Western Cordillera, Peru: ^{10}Be concentrations in modern sediments and terrace fills, *Journal of Geophysical Research:*
759 *Earth Surface*, 118(4), 2488–2499, <https://doi.org/10.1002/2013jf002837>, 2013.
- 760 Melnick, D.: Rise of the central Andean coast by earthquakes straddling the Moho, *Nature Geoscience*, 9(5), 401–407,
761 <https://doi.org/10.1038/ngeo2683>, 2016.



- 762 Miller, S. R., Sak, P. B., Kirby, E. and Bierman, P. R.: Neogene rejuvenation of central Appalachian topography: Evidence for
763 differential rock uplift from stream profiles and erosion rates, *Earth and Planetary Science Letters*, 369–370, 1–12,
764 <https://doi.org/10.1016/j.epsl.2013.04.007>, 2013.
- 765 Mishra, A. K., Placzek, C. and Jones, R.: Coupled influence of precipitation and vegetation on millennial-scale erosion rates
766 derived from ^{10}Be , *PLoS One*, 14(1), e0211325, <https://doi.org/10.1371/journal.pone.0211325>, 2019.
- 767 Mowll, W., Blumenthal, D. M., Cherwin, K., Smith, A., Symstad, A. J., Vermeire, L. T., Collins, S. L., Smith, M. D. and
768 Knapp, A. K.: Climatic controls of aboveground net primary production in semi-arid grasslands along a latitudinal gradient
769 portend low sensitivity to warming, *Oecologia*, 177(4), 959–969, <https://doi.org/10.1007/s00442-015-3232-7>, 2015.
- 770 Oeser, R. A., Stronck, N., Moskwa, L.-M., Bernhard, N., Schaller, M., Canessa, R., van den Brink, L., Köster, M., Brucker,
771 E., Stock, S., Fuentes, J. P., Godoy, R., Matus, F. J., Osés Pedraza, R., Osés McIntyre, P., Paulino, L., Seguel, O., Bader, M.
772 Y., Boy, J., Dippold, M. A., Ehlers, T. A., Kühn, P., Kuzyakov, Y., Leinweber, P., Scholten, T., Spielvogel, S., Spohn, M.,
773 Übernicker, K., Tielbörger, K., Wagner, D. and von Blanckenburg, F.: Chemistry and microbiology of the Critical Zone along
774 a steep climate and vegetation gradient in the Chilean Coastal Cordillera, *CATENA*, 170, 183–203,
775 <https://doi.org/10.1016/j.catena.2018.06.002>, 2018.
- 776 Owen, J. J., Amundson, R., Dietrich, W. E., Nishiizumi, K., Sutter, B. and Chong, G.: The sensitivity of hillslope bedrock
777 erosion to precipitation, *Earth Surface Processes and Landforms*, 36(1), 117–135, <https://doi.org/10.1002/esp.2083>, 2011.
- 778 Pelletier, J. D.: Fluvial and slope-wash erosion of soil-mantled landscapes: detachment- or transport-limited?, *Earth Surface
779 Processes and Landforms*, 37(1), 37–51, <https://doi.org/10.1002/esp.2187>, 2012.
- 780 Perron, J. T.: Climate and the Pace of Erosional Landscape Evolution, *Annual Review of Earth and Planetary Sciences*, 45(1),
781 561–591, <https://doi.org/10.1146/annurev-earth-060614-105405>, 2017.
- 782 Rossel, K., Aguilar, G., Salazar, E., Martinod, J., Carretier, S., Pinto, L. and Cabré, A.: Chronology of Chilean Frontal
783 Cordillera building from geochronological, stratigraphic and geomorphological data insights from Miocene intramontane-
784 basin deposits, *Basin Research*, 30, 289–310, <https://doi.org/10.1111/bre.12221>, 2018.
- 785 Routschek, A., Schmidt, J. and Kreienkamp, F.: Impact of climate change on soil erosion — A high-resolution projection on
786 catchment scale until 2100 in Saxony/Germany, *Catena*, 121, 99–109, <https://doi.org/10.1016/j.catena.2014.04.019>, 2014.
- 787 Sala, O. E., Parton, W. J., Joyce, L. A. and Lauenroth, W. K.: Primary Production of the Central Grassland Region of the
788 United States, *Ecology*, 69(1), 40–45, <https://doi.org/10.2307/1943158>, 1988.
- 789 Schaller, M. and Ehlers, T. A.: Limits to quantifying climate driven changes in denudation rates with cosmogenic
790 radionuclides, *Earth and Planetary Science Letters*, 248(1–2), 153–167, <https://doi.org/10.1016/j.epsl.2006.05.027>, 2006.
- 791 Schaller, M., Blanckenburg, F. von, Hovius, N., Veldkamp, A., van den Berg, M. W. and Kubik, P. W.: Paleoenvironmental Rates
792 from Cosmogenic ^{10}Be in a 1.3 Ma Terrace Sequence: Response of the River Meuse to Changes in Climate and Rock Uplift,
793 *The Journal of Geology*, 112(2), 127–144, <https://doi.org/10.1086/381654>, 2004.
- 794 Schaller, M., Ehlers, T. A., Lang, K. A. H., Schmid, M. and Fuentes-Espoz, J. P.: Addressing the contribution of climate and
795 vegetation cover on hillslope denudation, Chilean Coastal Cordillera (26°–38°S), *Earth and Planetary Science Letters*, 489,
796 111–122, <https://doi.org/10.1016/j.epsl.2018.02.026>, 2018.
- 797 Schmid, M., Ehlers, T. A., Werner, C., Hickler, T. and Fuentes-Espoz, J.-P.: Effect of changing vegetation and precipitation
798 on denudation – Part 2: Predicted landscape response to transient climate and vegetation cover over millennial to million-year
799 timescales, *Earth Surface Dynamics*, 6(4), 859–881, <https://doi.org/10.5194/esurf-6-859-2018>, 2018.
- 800 Seybold, H., Rothman, D. H. and Kirchner, J. W.: Climate’s watermark in the geometry of stream networks, *Geophysical
801 Research Letters*, 44(5), 2272–2280, <https://doi.org/10.1002/2016gl072089>, 2017.
- 802 Shobe, C. M., Tucker, G. E. and Barnhart, K. R.: The SPACE 1.0 model: A Landlab component for 2-D calculation of sediment
803 transport, bedrock erosion, and landscape evolution, *Geoscientific Model Development Discussions*, 1–38,
804 <https://doi.org/10.5194/gmd-2017-175>, 2017.
- 805 Slater, L. J. and Singer, M. B.: Imprint of climate and climate change in alluvial riverbeds: Continental United States, 1950-
806 2011, *Geology*, 41(5), 595–598, <https://doi.org/10.1130/g34070.1>, 2013.



- 807 Smith, B., Waarind, D., Arneth, A., Hickler, T., Leadley, P., Siltberg, J. and Zaehle, S.: Implications of incorporating N
808 cycling and N limitations on primary production in an individual-based dynamic vegetation model, *Biogeosciences*, 11(7),
809 2027–2054, <https://doi.org/10.5194/bg-11-2027-2014>, 2014.
- 810 Smith, M. D., Wilcox, K. R., Power, S. A., Tissue, D. T. and Knapp, A. K.: Assessing community and ecosystem sensitivity
811 to climate change – toward a more comparative approach, *Journal of Vegetation Science*, 28(2), 235–237,
812 <https://doi.org/10.1111/jvs.12524>, 2017.
- 813 Starke, J., Ehlers, T. A. and Schaller, M.: Latitudinal effect of vegetation on erosion rates identified along western South
814 America, *Science*, 367(6484), 1358, <https://doi.org/10.1126/science.aaz0840>, 2020.
- 815 Tucker, G., Lancaster, S., Gasparini, N. and Bras, R.: The channel-hillslope integrated landscape development model
816 (CHILD), in: *Landscape erosion and evolution modeling*, Springer, Boston, MA, USA, 349–388, 2001.
- 817 Tucker, G. E.: Drainage basin sensitivity to tectonic and climatic forcing: implications of a stochastic model for the role of
818 entrainment and erosion thresholds, *Earth Surface Processes and Landforms*, 29(2), 185–205,
819 <https://doi.org/10.1002/esp.1020>, 2004.
- 820 Turowski, J. M., Lague, D., Crave, A. and Hovius, N.: Experimental channel response to tectonic uplift, *Journal of Geophysical*
821 *Research: Earth Surface*, 111(F3), n/a-n/a, <https://doi.org/10.1029/2005jf000306>, 2006.
- 822 Werner, C., Schmid, M., Ehlers, T. A., Fuentes-Espoz, J. P., Steinkamp, J., Forrest, M., Liakka, J., Maldonado, A. and Hickler,
823 T.: Effect of changing vegetation and precipitation on denudation – Part 1: Predicted vegetation composition and cover over
824 the last 21 thousand years along the Coastal Cordillera of Chile, *Earth Surface Dynamics*, 6(4), 829–858,
825 <https://doi.org/10.5194/esurf-6-829-2018>, 2018.
- 826 Whipple, K. X.: The influence of climate on the tectonic evolution of mountain belts, *Nature Geoscience*, 2(10), 730–730,
827 <https://doi.org/10.1038/ngeo638>, 2009.
- 828 Willgoose, G., Bras, R. L. and Rodriguez-Iturbe, I.: A coupled channel network growth and hillslope evolution model: 1.
829 Theory, *Water Resources Research*, 27(7), 1671–1684, <https://doi.org/10.1029/91WR00935>, 1991.
- 830 Xia, J., Chen, J., Piao, S., Ciais, P., Luo, Y. and Wan, S.: Terrestrial carbon cycle affected by non-uniform climate warming,
831 *Nature Geoscience*, 7(3), 173–180, <https://doi.org/10.1038/ngeo2093>, 2014.
- 832 Yang, Y., Fang, J., ma, W. and Wang, W.: Relationship between variability in aboveground net primary production and
833 precipitation in global grasslands. *Geophysical Research Letters*, *Geophysical Research Letters - GEOPHYS RES LETT*, 35,
834 <https://doi.org/10.1029/2008GL035408>, 2008.
- 835 Yanites, B. J. and Ehlers, T. A.: Global climate and tectonic controls on the denudation of glaciated mountains, *Earth and*
836 *Planetary Science Letters*, 325–326, 63–75, <https://doi.org/10.1016/j.epsl.2012.01.030>, 2012.
- 837 Zhang, Y., Xiao, X., Guanter, L., Zhou, S., Ciais, P., Joiner, J., Sitch, S., Wu, X., Nabel, J., Dong, J., Kato, E., Jain, A. K.,
838 Wiltshire, A. and Stocker, B. D.: Precipitation and carbon-water coupling jointly control the interannual variability of global
839 land gross primary production, *Scientific Reports*, 6(1), 39748, <https://doi.org/10.1038/srep39748>, 2016.

840